Title

Use of multiple tools including lead isotopes to decipher sources of ozone and reactive mercury to urban and rural locations in Nevada, USA

Authors

Pierce, Ashley M

Gustin, Mae Sexauer

Christensen, John N

et al.

Publication Date

2018-02-01

DOI

10.1016/j.scitotenv.2017.08.284

Peer reviewed

Use of multiple tools including lead isotopes to decipher sources of ozone and reactive mercury to urban and rural locations in Nevada, USA

Ashley M. Pierce[a,*], Mae Sexauer Gustin[a,*], John N. Christensen[b], S. Marcela Loría-Salazar[c]

*Corresponding author: ash.pie4@gmail.com; mgustin@cabnr.unr.edu

[a]Department of Natural Resources and Environmental Sciences, University of Nevada Reno, Reno, NV, USA 89557

[b]Energy Geosciences Division, Lawrence Berkeley National Laboratory, Berkeley, CA, USA 94720

[c]Atmospheric Science Program, Department of Physics, University of Nevada, Reno, Nevada, USA

Abstract:

Particulate matter (<2.5 μm in diameter) samples were collected in 2014 and 2015 for 24 h reactive mercury concentrations and lead isotopes to determine sources of pollution to three sites in Nevada, USA. Two adjacent sites were located on the western edge of Nevada (Reno, urban, 1370 m and Peavine Peak, rural, high elevation, 2515 m); the third location was ~485 km east in rural Great Basin National Park (2061 m). Ambient reactive mercury (gaseous oxidized mercury + particulate bound mercury) was collected on cation exchange membranes simultaneously with lead samples, collected using Teflon membranes. A Tekran total mercury system (Model 2600) was used for analyses of CEM filters for total mercury. Lead isotope samples were analyzed with a multi-collector inductively coupled plasma mass spectrometer (Neptune).

Lead isotopic ratios have previously been used to identify trans-Pacific lead sources based on the 206/207 and 208/207 lead ratios. Influence from trans-Pacific air masses was higher from March to June associated with long-range transport of pollutants. Spring months are well known for increased transport across the Pacific; however, fall months were also influenced by trans-Pacific air masses in this study.

Western North American background ozone concentrations have been measured and modeled at 50 to 55 ppbv. Median ozone concentrations at both rural sites in Nevada were within this range. Sources leading to enhancements in ozone of 2 to 18 ppbv above monthly medians in Nevada included emissions from Eurasia, regional urban centers, global, and regional wildfires, resulting in concentrations close to the US air quality standard.

Negative correlations between reactive mercury and percent Asian lead, Northern Eurasia trajectories and East Asia trajectories indicated reactive mercury concentrations at the two high elevations sites were produced by oxidants from local, regional, and marine boundary layer sources. At the high elevation locations, ozone was derived from pollutants being transported in the free troposphere that originate around the globe; however, Eurasia and Asia were the dominant sources to the Western USA.

Keywords:

$PM_{2.5}$, MC-ICPMS, long-range transport, pollution sources, complex terrain

50

1. Introduction:

Determining sources of pollution in complex terrains, such as the Western United States of America (USA), is difficult due to a combination of complicated meteorological conditions (e.g. complex planetary boundary layer processes, El Niño/Southern oscillation, and jet streams), stratospheric-tropospheric exchange (STE), and long-range transport of air masses. Moreover, determining sources of ozone (O_3) is particularly complex as it is a secondary pollutant that forms downwind of primary pollution sources. These factors provide multiple challenges for regulators given the task of determining measures for meeting the National Ambient Air Quality Standard (NAAQS) for O_3 in the Western USA (Cooper et al., 2015). This research was conducted with the purpose of understanding sources of O_3 and reactive mercury (RM) to Nevada, USA in 2014 and 2015, using lead (Pb) isotopes and a suite of other measurements.

In the troposphere, O_3 is a harmful oxidant that has detrimental effects on materials (such as rubber), leaves and therefore crops and forests, and mucous membranes and respiratory tissues in organisms (U.S. EPA, 2013). Ozone also affects climate change because it absorbs infrared radiation (Finlayson-Pitts and Pitts Jr, 2000a; Finlayson-Pitts and Pitts Jr, 2000b). The current USA Environmental Protection Agency (EPA) NAAQS is set to 70 parts per billion (ppbv) 8 h maximum (max) daily average (MDA8) concentration and determined based on the 3-year running average of the annual fourth-highest MDA8 (called the design value, U.S. EPA, 2013). The European Union standard is set to 60 ppbv MDA8 with 25 exceedance days averaged over 3 years (European Commission, 2016). Washoe County, in which two field sites in this study, Reno and Peavine Peak, reside is out of attainment for O_3 for the 2014 to 2016 averaging years, due to several large fires during this time (EPA, 2017).

Spring and summer maximums of O_3 are often observed across the Northern Hemisphere due to increased photochemical reactions with accumulated NO_x, increased STE, and long-range transport of precursors from other continents (Prinn, 2014; Vingarzan, 2004; Wilkening et al., 2000; Zhang et al., 2014). Springtime O_3 concentrations in mid-latitudes are also influenced by El Niño/Southern Oscillation, especially during strong El Niño events in which O_3 is transported from the tropics to the extra-tropics (Lin et al., 2012; Rieder et al., 2013). Stratospheric-tropospheric exchange is greatest over North America in the spring, due to increased storm activity and a low tropopause allowing for better vertical down mixing from the stratosphere

(Ambrose et al., 2011; Dempsey, 2014; Fine et al., 2015a; Johnson and Viezee, 1981; Langford et al., 2012; Langford et al., 2015a; Langford et al., 2015b; Langford, 2017; Lin et al., 2015; Stohl et al., 2000; Tang and Prather, 2010; Viezee et al., 1983; Vingarzan, 2004). Summer in the Western USA also means increased wildfires, which can increase summer mean MDA8 O_3 by 0.3-1.5 ppbv with episodic increases of 10-20 ppbv (Lu et al., 2016).

Research has demonstrated that long-range transport of gases and particulate matter from Eurasia, impacts air quality in the Northeast Pacific and North America (Bertschi and Jaffe, 2005; Christensen et al., 2015; Ewing et al., 2010; Fine et al., 2014; Jaffe et al., 1999; Jaffe et al., 1997; Jaffe et al., 2003; Lin et al., 2012; Price et al., 2004; Teakles et al., 2017; VanCuren, 2003; VanCuren et al., 2005; Weiss-Penzias et al., 2007; Weiss-Penzias et al., 2006). Trans-Pacific, atmospheric pollutants are predominant in the spring due to increased storm, and frontal activity in Eurasia, facilitating transport of air across the Pacific (Cooper et al., 2010; Knowland et al., 2015; Kunz and Speth, 1997; Vingarzan, 2004). Increased fires in Eurasia in the spring also add pollutants to the atmosphere for trans-Pacific transport (Cooper et al., 2010; Vingarzan, 2004). In the Western USA, trans-Pacific input has reportedly influenced background and surface O_3 concentrations by 3 to 15 ppbv and contributed to exceedances of 70 ppbv springtime MDA8 O_3 concentrations (Fiore et al., 2002; Fiore et al., 2014; Jacob et al., 1999; Jaffe et al., 2004; Jaffe et al., 2003; Langford et al., 2015b; Lin et al., 2012; Vingarzan, 2004). This influence will increase as Asian countries continue to develop, affecting Western USA, rural O_3 by ~0.5 ppbv/yr (Christensen et al., 2015; Cooper et al., 2010; Gratz et al., 2015). Total annual area burned of boreal fires in Eurasia has also been shown to significantly impact O_3 and CO summer seasonal means, explaining 42 to 86% inter-annual variability across sites in Western North America (Jaffe et al., 2004).

Ashley 8/14/17 1:40 PM
Comment: Th

Ashley 8/14/17 1:40 PM
Comment:

Ashley 8/14/17 1:40 PM
Comment: These studies are specifically background and surface ozone, not baseline.

Higher O_3 concentrations have been measured at high elevation sites in Western USA, compared to nearby lower elevations, due to layers of polluted trans-Pacific air, lofting of pollution produced in California into the free troposphere, and stratospheric intrusions (Brodin et al., 2010; Burley and Bytnerowicz, 2011; Fine et al., 2015a; Fine et al., 2015b; Fiore et al., 2002; Gustin et al., 2015b; Jaffe et al., 2003; Lin et al., 2012; VanCuren, 2015; Vingarzan, 2004). Sites in California and Nevada have shown a strong relationship between site altitude and maximum (max) 1 h O_3 indicating an increase of 13 ppbv for every km of elevation in the summer, and 7 to 10 ppbv/km in other seasons (Fine et al., 2015b). Previous data and models indicated that high

elevation, rural sites in Western USA, such as Great Basin National Park, NV, exceeded the NAAQS design value concentration and will continue to exceed if sources and processes remain constant or increase (Fine et al., 2015a; Lin et al., 2012).

Mercury (Hg) is a global pollutant and neurotoxin that can negatively affect ecosystems as it bio-accumulates in the food web. The Global Mercury Assessment, updated in 2015, estimated that ~40% of global anthropogenic Hg emissions come from East and Southeast Asia generally in the form of gaseous elemental Hg (GEM, AMAP/UNEP, 2015; Jaffe et al., 2005). Reactive Hg (RM), considered to be gaseous oxidized Hg (GOM) and particulate bound Hg (PBM), has a shorter residence time in the boundary layer (a day to a week, Schroeder and Munthe, 1998) compared to GEM (6 months to a year). GEM is considered a global pollutant that is transported far from sources and can then be oxidized by a variety of gases and deposited (Weiss-Penzias et al., 2003). RM will undergo reactions or deposit close to sources and can also be formed in dry upper altitude air due to photo-oxidation of GEM near the tropopause and in the stratosphere (Lyman and Jaffe, 2012). Positive correlations between RM and O_3 have been previously observed and interpreted as photo-oxidation in upper altitude air (Weiss-Penzias, 2015). It has also been demonstrated that RM dry deposition is higher at higher elevation sites in California and Nevada (Huang and Gustin, 2015).

The Minamata Convention, adopted in 2013, commits signatories to better understanding atmospheric Hg sources and to reducing emissions to the environment (UNEP, 2017). RM measurements are currently under review due to uncertainties in widely used, commercially available, measurement methods (Gustin et al., 2015a; Gustin et al., 2013; Huang and Gustin, 2015; Huang et al., 2013; Jaffe et al., 2014). A better understanding of the atmospheric cycling of Hg, the main pathway into environments, is necessary for fulfilling the goals of the Minamata Convention.

Lead isotope analysis has previously been used to identify sources of pollution (Ewing et al., 2010), and specifically O_3, to the Western USA (Christensen et al., 2015). Using Pb isotopic ratios in particulate matter (PM), collected on filters, provides a means of identifying sources. As air masses move away from sources, pollutant chemistry changes but Pb isotope ratios do not. There are systematic, geographic differences in Pb isotopic compositions of the four stable isotopes; ^{208}Pb (52%), ^{207}Pb (23%), ^{206}Pb (24%), and ^{204}Pb (1%), of which the three heaviest are produced from radioactive decay that occurs over billions of years (Komárek et al., 2008).

Studies have shown that Pb associated with Asian aerosols has an isotopic composition distinct from Pb in Western North America (Bollhöfer and Rosman, 2002; Ewing et al., 2010), specifically, a higher proportion of ^{208}Pb in $^{208}Pb/^{207}Pb$ versus $^{206}Pb/^{207}Pb$ isotopic ratios (Bollhöfer and Rosman, 2001). Analysis of PM collected on filters for Pb isotope ratios can therefore elucidate where air masses originate. The NAAQS design value for Pb is 0.15 μg m^{-3} in total suspended particles averaged over 3 months.

From 2001 to 2009, coal combustion was the largest emission source of Pb in China (Li et al., 2012). The USA is a net exporter of coal, of which ~20% goes to Asia (2014: exports = 88 billion kg, imports = 10 billion kg, 2015: exports = 67 billion kg, imports = 10 billion kg of coal, U.S. Energy Information Administration, 2017). Although imported coal is a small amount of the total coal used in the USA (<2%) or in Asia (<0.5%), transport in isolated parcels of air (Fine et al., 2015b) may complicate the Pb isotopic signature by adding isotopes that are not representative of the source region (U.S. Energy Information Administration, 2017). In addition, some coals are low in Pb and will therefore, not have discernable isotopic signatures.

In 2011, data collection for the Nevada Rural Ozone Initiative (NVROI) was initiated. The goal of this study was to understand sources of O_3 to the complex terrain and rural areas of the Western USA (Gustin et al., 2015b). This component of the project investigated the use of aerosol concentration and chemistry to understand sources of air masses. Three of the NVROI sites housed modified Teledyne Advanced Pollution Instrumentation (TAPI) particulate measurement systems to quantify particulate matter <2.5 μm in diameter ($PM_{2.5}$), RM (GOM+PBM) concentrations, and Pb concentration and isotopes. This research required multiple sources of data to identify sources of air masses to Nevada in summer through fall 2014 and spring to fall 2015. Given that Nevada, with the exception of Reno and Las Vegas, is a rural state with complex terrain, high elevation, and limited sources of O_3 precursors, we hypothesized a component of the O_3 and RM was from long-range transport across the Pacific Ocean.

2. Site descriptions:

Data were collected at three sites with two sites being simultaneously operated at a time. The goal was to understand sources of O_3 to individual locations. More detailed site descriptions are provided in Fine et al. (2015a), Gustin et al. (2015b), Miller et al. (2015), and in Table 1. The Nevada Agricultural Experiment Station Greenhouse Facility (UNRG; 1371 m, Table 1) is

located at the Valley Road field labs and Greenhouse complex of the University of Nevada, Reno (UNR) in the topographic bowl of the Reno/Sparks metropolitan area. Data collected from April 2014 to October 2015 were used from this site. The Peavine Peak (PEAV; 2515 m, Table 1) site is situated above the tree line at the peak summit. PEAV is located just east of the Sierra Nevada Mountains (~15 km) and northwest of Reno (~12 km). Data from June to November 2014 were used from this site. The third site, Great Basin National Park (GBNP; 2060 m, Table 1), is located ~485 km due east of Reno in eastern NV at the Utah border. The measurement station is located on the east side of the Snake Range in a forested area, mainly pinyon-juniper, near the Lehman Visitor Center where two canyons merge in a slight topographic bowl. Data were collected from March to October 2015 at this location.

Table 1: Measurement sites and the measurements made at each. Abbreviations are explained under the table with sample resolution in parentheses.

Site	Code	Elevation (m asl)	Measurements	Other	Latitude (N)	Longitude (W)
Great Basin National Park, NV, USA	GBNP	2060	TAPI, CO, SO_2, NO_x, NO_y, Met, E-BAM	IMPROVE, CASTNET	39.0050	114.2161
Nevada Agricultural Experiment Station Greenhouse Facilities, Reno. NV, USA	UNRG	1371	TAPI, O_3, CO, NO_x	WCAQ (Reno3), WRCC	39.5374	119.8044
Peavine Peak, Reno, NV, USA	PEAV	2515	TAPI, O_3, CO, Met		39.5895	119.9290

asl – above sea level
CASTNET - Clean Air Status and Trends Network (1 h)
CO – carbon monoxide (1 h)
E-BAM – Environmental Beta Attenuation Monitor ($PM_{2.5}$, 1 h)
IMPROVE - Interagency Monitoring of Protected Visual Environments (24 h once every 3 days)
Met – meteorological data (1 h)
NO – nitrogen oxide (1 h)
NOx – nitrogen oxide compounds (1 h)
NOy – total reactive nitrogen (1 h)
SO_2 – sulfur dioxide (1 h)
TAPI – Teledyne Advanced Pollution Instrumentation Model 602 Beta^{Plus} $PM_{2.5}$ monitor (24 h)
WCAQ – Washoe County Air Quality (1 h)
WRCC – Western Regional Climate Center (1 h)

3. Methods:

Data from multiple platforms (described below) were collected for each site at hourly, 24 h, or once daily resolution and compared at 24 h, 1 h max values, or 8 h max running averages. Filters collected using two TAPI Beta^{Plus} particulate measurement systems for $PM_{2.5}$ samples were post-processed for Pb isotopic composition and RM concentrations. Statistical tests were performed to illustrate differences between sites and to identify significant relationships. Trajectory analysis were applied to identify possible sources of air masses. Specific periods based on exceedances of monthly medians were then chosen for more in depth analysis.

3.1 Teledyne Advanced Pollution Instrumentation (TAPI) Beta^{Plus} Particulate Monitor

Two TAPI Beta^{Plus} particulate measurement systems (Model 602, San Diego, CA, USA) were used to collect $PM_{2.5}$. RM concentrations and compounds, and Pb concentrations and isotope ratios were determined. The TAPI Beta^{Plus} particulate measurement system was modified to collect RM on 47 mm cation exchange membranes (CEM; Pall Corporation, PN: MSTGS3R) and Pb on 47 mm Teflon (Pall Corporation, PN: EW-36329-08) for 24 h. Mass concentration was measured using beta attenuation, leaving filters intact and available for further processing (see SI and Gustin (2016) for more detail).

Pierce and Gustin (2017) showed that $PM_{2.5}$ measurements using CEM filters were statistically similar to Federal Reference (FRM) and Federal Equivalent methods (FEM). At 24 h the TAPI Beta^{Plus} particulate measurement system has a $PM_{2.5}$ detection limit of 0.3 $\mu g\ m^{-3}$ (TAPI, 2012).

3.2 Lead isotope analysis

Teflon filters were processed at Lawrence Berkeley National laboratory (LBNL) in class 100 laminar fume hoods, following Ewing et al. (2010) and Christensen et al. (2015) and analyzed on with a multi-collector inductively coupled plasma mass spectrometer (MC-ICPMS Neptune). See SI for details on sample processing.

Percent of Pb attributed to Asia was calculated using methodology developed in Ewing et al. (2010) and applied in Christensen et al. (2015). Wintertime aerosol samples from the Chabot Observatory in California define the "California Array" (blue line and blue squares, Fig. 1, slope = 1.22). Chinese aerosol and loess data define the "Asia Array" (black line and black triangles and squares, Fig 1, slope = 1.09). The horizontal divergence ($\Delta^{208}Pb$) from California $^{208}Pb/^{207}Pb$ isotope data towards Asian $^{208}Pb/^{207}Pb$ isotope data at a specific observed $^{206}Pb/^{207}Pb$ isotope value is calculated. The $\Delta^{208}Pb$ is then divided by the total distance between the two arrays to determine the percent of the Pb that can be attributed to Asian sources (Ewing et al., 2010). Data from previous studies collected from aerosol and ore samples were used to compare to samples collected in this study. Aerosol samples from different years may have differing isotope ratios over time and direct isotopic composition comparison of ores to aerosols, due to source and

239 supplier differences, is difficult, however these provide an estimate of isotopic ratios in different
240 areas.
241
242 *3.3 Ozone*
243 Hourly O_3 concentrations were measured at all three sites using UV absorption
244 instruments. O_3 measurements at PEAV were made using a TAPI T400E UV absorption O_3
245 analyzer. UNRG had a Thermo 49i (Thermo Fisher Scientific, Inc. Franklin, MA, USA). When
246 O_3 data were missing from UNRG it was supplemented with data from a TAPI 400E at the Reno
247 site (Reno3, site ID: 32-031-0016, 301A State St. Reno) of Washoe County Air Quality
248 Management (WCAQ). At GBNP, O_3 data were collected using a TAPI T400E UV absorption
249 O_3 analyzer operated by the Nevada Department of Environmental Protection (NDEP) and a
250 Thermo 49c operated by the National Park Service (NPS) Clean Air Statuses and Trends
251 Network (CASTNET).
252 WCAQ and UNRG data were statistically different (ANOVA $p<0.05$), but positively
253 correlated ($r^2 = 0.72$, $p<0.05$ for O_3), this is due to distance from a highway (manuscript in
254 preparation). Due to the positive correlation, variations in daily means compared to monthly
255 medians at WCAQ reflect the overall trends in the valley housing Reno, if not the specific
256 concentrations at UNRG, and were used to supplement when UNRG data were unavailable. At
257 GBNP, CASTNET and NDEP O_3 were statistically similar (ANOVA $p>0.05$, $r^2 = 0.93$, $p<0.05$),
258 CASTNET data supplemented periods when NDEP data were not available.
259 Here we discuss MDA8 as the max 8 h average for a day, but do not compare to the
260 MDA8 NAAQS design value (3-year running average of the annual fourth highest MDA8).
261 Ozone data were compiled and compared with other data as 24 h daily averages, MDA8 values
262 for each day, and the max 1 h O_3 values for each day. The second two values are more likely to
263 capture transport events that may occur within a shorter time scale than a 24 h daily average and
264 are not affected by the smoothing effect that 24 h daily averages have on concentrations (Fine et
265 al., 2015b; Langford, 2017).
266
267 *3.4 Mercury*

CEM filters were digested and then analyzed using an automated Tekran 2600 Hg analyzer following EPA method 1631 for total Hg concentrations. The RM method detection limit was 0.3 ng. See SI and Pierce & Gustin (2016) for further detail.

3.5 Auxiliary Gas and Meteorological data

Measured auxiliary gases are listed in Table 1 and described in Fine et al. (2015a), Gustin et al. (2015b), and Miller et al. (2015), as is meteorological data. All gas instruments at PEAV and GBNP (NDEP) were trace level. Vertical potential temperature from atmospheric balloon soundings were used to calculate the height of the atmospheric boundary layer, termed the atmospheric boundary layer height (ABLH). This data came from soundings released from the National Weather Service in Reno, NV (REV) at 16:00 PST. Late afternoon vertical profiles illustrate the maximum height that the ABLH can potentially reach. Data collected by other organizations, including Washoe County Air Quality Management (WCAQ), Western Regional Climate Center (WRCC), Interagency Monitoring of Protected Visual Environments (IMPROVE), and the Clean Air Status and Trends Network (CASTNET) monitoring networks were also used.

3.6 Hybrid Single Particle Lagrangian Integrated Trajectory (HYSPLIT) Model

The NOAA Air Resources Lab HYSPLIT v.4 model (Draxler and Hess, 1997) using the 1° Global Data Assimilation System (GDAS, 23 vertical layers) from the National Center for Environmental Prediction (NCEP, http://ready.arl.noaa.gov/archives.php) was used to compile 240 h back trajectories from all three sites. Back trajectories were initiated every 4 h (00:00, 04:00, 08:00, 12:00, 16:00, 20:00 PST) from 9 points within a 0.5°x0.5° horizontal grid centered on each site with four arrival heights (500, 1000, 1500, 2000 m agl), generating 216 trajectories a day, or 51,840 hourly trajectory points. Back trajectories give a general indication of a source region and are less useful for vertical motion: however, generating large numbers of trajectories gives a general representation of air mass transport (Stohl et al., 2002; Stohl et al., 2003; Weiss-Penzias et al., 2006).

Trajectory residence times (TRT) were calculated as the percent of the total hourly trajectory points (out of 240 h) that a trajectory resided in a 3 dimensional source box. There were five defined source boxes (see TOC graphic and SI Table 1): Northern Eurasia (N.

Eurasia), East Asia (E. Asia), San Francisco, CA (SF), Los Angeles, CA (LA), and Las Vegas, NV (LV). Trajectory resident times for air parcels occurring <3 km, total (<10 km), and >3 km were used for N. Eurasia and E. Asia source boxes. Due to difficulties the HYSPLIT model has with resolving boundary layer to free troposphere exchange in distant source boxes, <3 km trajectory residence times were used to represent air masses in contact with these source regions (Stohl, 1998; Weiss-Penzias et al., 2006). Trajectory points <1 km over SF, LA, and LV were used as indicators of sources from those areas, while trajectory residence times >3 km over SF was used as an indicator of transport from over the marine boundary layer (MBL) and of high-altitude air where China is the dominant source of O_3 precursors (Cooper et al., 2011). TRT percentages were used in the Pearson correlation (R), discussed in section 3.8, to determine influence from the different source boxes on the three measurement sites.

3.7 Moderate Resolution Imaging Spectroradiometer (MODIS)

Fire Radiative Power (FRP) retrievals from the Terra (morning overpass) and Aqua (afternoon overpass) satellites were used as an indicator of fire frequency and intensity from the N. Eurasia source box and from Western North America including Canada (latitude: 30 to 60 and longitude: -124 to -100 degrees). FRP retrievals from the two satellites were averaged for each day. Daily number (n), minimum (min), maximum (max), mean, standard deviation, and median were calculated for the sample periods. FRP days were chosen based on the first day and last day during a 10-day back trajectory in which a trajectory passed through the N. Eurasia source box or Western North America. If a trajectory was within the Western North America bounds for 240 hours, the middle day in that time was used.

3.8 Data analyses:

Data were processed using Python, the R program, Matlab, and Excel. ESRI ArcGIS was used for map creation. Monthly means, daily means, and maximums were calculated from hourly data for each sample period. Data were used if >50% of the data were available. When NVROI data was unavailable they were supplemented by other data sources (WCAQ, CASTNET). Monthly means were compared using ANOVA (two factor without replication) to determine if the two sites differed. Pearson correlation was used to assess correlation and significance for variables for the sample period at each site and for observations at the sites for days with Pb data

using daily means for each variable. Statistical tests were considered significant at $\alpha<0.05$, unless otherwise noted.

4. Results:

During both study periods, median $PM_{2.5}$ concentrations were higher at the urban location than at PEAV or GBNP (Table 1). Median concentrations of RM were higher at GBNP than UNRG. The higher elevation locations (PEAV and GBNP) both had higher 24 h average O_3 compared to UNRG. PEAV had higher max 1 h and MDA8 O_3 than UNRG. Average Δ208 Pb for all samples was 7.2±4.7 with an average uncertainty of 0.12±0.080, which corresponds to an average % Asian Pb of 29±19% and an average uncertainty of 0.47±0.32%. Uncertainty for individual measurements can be found in SI Table 2. Pb concentrations were always less than the concentration used for the NAAQS design value (0.15 μg m^{-3} or 150 ng m^{-3}).

Table 2: Sample statistics for a) PEAV and UNRG June to November 2014 and GBNP and UNRG March to October 2015 and b) for all sites June-October. Site means ± one standard deviation, medians, number of days (n), and range of data.

a) All data

Site	Statistics	$PM_{2.5}$ (μg m^{-3})	RM (pg m^{-3})	O_3 (ppbv)	Max 1 h O_3 (ppbv)	MDA8 O_3 (ppbv)	Total Pb (ng m^{-3})	Asian Pb (ng m^{-3})	% Asian Pb
PEAV 2014	Mean ± StDev	5.94±6.1	43±27	48±7.2	56±8.4	53±7.6	0.34±0.15	0.090±0.089	26±15
	Median (n)	4.9 (141)	38 (153)	49 (158)	56 (158)	53 (158)	0.32 (19)	0.065 (19)	23 (19)
	Range	0.0-42	1.4-147	25-69	40-80	39-78	0.13-0.72	0.0025-0.38	0.51-58
UNRG 2014	Mean ± StDev	8.9±7.7	41±23	26±10	46±14	40±12	0.76±0.61	0.24±0.43	24±17
	Median (n)	7.1 (133)	34 (132)	26 (117)	48 (117)	42 (117)	0.60 (19)	0.11 (19)	21 (19)
	Range	0.0-63	8.4-106	2.6-49	7.4-77	13-65	0.20-3.1	-0.024-1.9	-2.4-63
GBNP 2015	Mean ± StDev	4.4±2.9	45±33	48±7.2	56±8.0	53±7.5	0.26±0.13	0.081±0.071	31±22
	Median (n)	3.8 (171)	38 (174)	47 (169)	54 (169)	52 (169)	0.25 (23)	0.062 (23)	30 (23)
	Range	0.30-21	2.5-134	32-81	35-82	35-82	0.12-0.70	-0.069-0.27	-28-74
UNRG 2015	Mean ± StDev	6.7±3.9	30±24	36±11	58±12	52±12	1.5±1.2	0.69±0.88	35±23
	Median (n)	6.1 (162)	22 (154)	34 (194)	57 (194)	50 (194)	1.1 (11)	0.34 (11)	25 (11)
	Range	1.7-35	1.5-121	15-71	29-92	25-85	0.35-4.4	0.032-2.9	9.0-74

b) June-October

Site	Statistics	$PM_{2.5}$ (μg m^{-3})	RM (pg m^{-3})	O_3 (ppbv)	Max 1 h O_3 (ppbv)	MDA8 O_3 (ppbv)	Total Pb (ng m^{-3})	Asian Pb (ng m^{-3})	% Asian Pb
PEAV 2014	Mean ± StDev	10±6.6	48±26	50±6.6	58±8.1	55±7.5	0.33±0.13	0.070±0.060	23±14
	Median (n)	5.3 (105)	42 (117)	50 (119)	57 (119)	54 (119)	0.33 (16)	0.06 (16)	20 (16)
	Range	0.80-42	1.9-140	34-69	42-80	39-78	0.13-0.63	0.0-0.26	0.51-58
UNRG 2014	Mean ± StDev	9.6±8.7	48±22	27±9.9	47±15	41±13	0.62±0.24	0.13±0.12	21±15

	Median (n)	7.4 (98)	44 (98)	29 (86)	48 (86)	42 (86)	0.59 (16)	0.10 (16)	21 (16)
	Range	0.0-63	8.4-106	8.9-49	19-77	14-65	0.20-1.0	-0.024-0.40	-2.4-47
GBNP 2015	**Mean ± StDev**	4.76±3.4	64±28	48±7.9	56±8.7	54±8.2	0.25±0.090	0.080±0.055	32±18
	Median (n)	4.1 (107)	59 (107)	47 (120)	54 (120)	52 (120)	0.26 (19)	0.062 (19)	26 (19)
	Range	1.1-21	17-134	32-81	35-82	35-82	0.12-0.46	0.022-0.21	6.68-74
UNRG 2015	**Mean ± StDev**	7.9±5.1	50±20	32±6.8	53±9.6	46±7.9	1.2±0.88	0.42±0.56	27±21
	Median (n)	6.7 (73)	49 (73)	31 (122)	53 (122)	46 (122)	0.82 (8)	0.24 (8)	21 (8)
	Range	2.7-35	21-121	19-44	34-85	29-65	0.35-2.4	0.032-1.7	9.0-74

GBNP – Great Basin National Park, NV, USA
Max 1 h O_3 – maximum 1 h average of each day
MDA8 O_3 – maximum daily average (8 h) for each day
O_3 – ozone
ppbv – parts per billion by volume
Pb - lead.
PEAV – Peavine Peak, Reno, NV, USA

$PM_{2.5}$ – particulate matter <2.5 μm in diameter

RM – reactive Hg
UNRG – University of Nevada, Reno, Greenhouse, USA

4.1 PEAV and UNRG 2014

During summer and fall (June to November 2014) when TAPI Beta^{Plus} particulate measurement systems were located at UNRG and at PEAV, O_3 monthly means and monthly MDA8 O_3 means were statistically higher at PEAV for all months. $PM_{2.5}$ and RM monthly means were not statistically different between the two sites. Chemical composition of RM (except for mid-to-late June) at UNRG were primarily N and S compounds, while at PEAV compounds were primarily halogen based Hg compounds with periodic appearances of Hg-O, nitrogen-, and sulfur-based compounds, indicating the sites were often isolated from each other.

Daily $PM_{2.5}$ mass concentrations were statistically higher at UNRG. CO monthly means were lower at PEAV. Percent Asian Pb for the two sites was similar, median Pb mass concentration was higher at UNRG. Wind speed monthly means were higher at PEAV. Monthly mean temperature was lower at PEAV, while RH monthly means were not statistically different between the two sites. These comparisons reflect the fact that PEAV is a high elevation location impacted by the free troposphere and that UNRG is adjacent to a highway, where increased levels of $PM_{2.5}$, Pb, and other pollutants (e.g. CO, NO_x, SO_2) are experienced.

Diel patterns of CO at PEAV (SI Fig. 1) indicate upslope convective mixing; increasing CO by ~60 ppbv in the afternoon. There was a small increase in O_3 (by ~2 ppbv) at this time as well. Positive correlation between O_3 and <1 km trajectories from San Francisco and negative

correlation with RH indicate that for this period, regional air from the west (prevailing wind direction) transported O_3 (SI Tables 3-6). Positive correlations between O_3 and ABLH and the diel patterns indicate impacts from upslope flow of pollutants from Reno, NV as the valley warmed (SI Fig. 1). However, given the small increase in O_3 (3%) the Reno/Sparks valley was not the primary source. Long-range transport and southern Nevada did not increase daily averages of O_3. Max 1 h and MDA8 O_3 often occurred with increased pollutants ($PM_{2.5}$ and CO), and drier, high, fast moving conditions, indicating long-range transport events occurred at a shorter time scale than 24 h.

RM at PEAV (SI Table 3) was positively correlated with O_3 and negatively correlated with N. Eurasia trajectories. This indicates the importance of local and regional sources of oxidants for formation. The >3 km trajectories from San Francisco and halogenated RM species ($HgBr_2$ and $HgCl_2$) measured at PEAV indicate that reactions in the marine boundary layer during this time influenced this site (Gustin et al., 2016; Timonen et al., 2013). Positive correlations between O_3 (daily average, max 1 h, MDA8 [$p<0.1$]), temperature, pressure, and ABLH also indicate that local sources could periodically influence RM, bringing up pollutants from the Reno/Sparks valley.

For the days with Pb isotope analysis at PEAV (19 days, SI Tables 7-11), % Asian Pb was correlated with trajectories from E. Asia; however, this was not correlated with O_3. Total Asian Pb and % Asian Pb were derived using data from Asia (China), a large emitter of Pb due to industrial processes, so the positive correlation with E. Asia trajectories is reasonable. This correlation and positive correlations with O_3 demonstrates that Asia was a significant source of Pb to this high elevation site. Pb isotopes measured at PEAV during this time were located on the California Array and on a mixing line that had a slope of 0.92 ($r^2 = 0.90$) and intercepted and overlapped ores from Russia, Mongolia, and Kazakhstan (Fig. 1a). Based on meteorology, other sites in Nevada will also experience significant amounts of Pb from Asia (Christensen et al., 2015; Gustin et al., 2015b). RM was not correlated with % Asian Pb further supporting regional impacts of oxidants on RM concentrations and formation.

John Christensen 8/18/17 9:33 AM
Comment: Didn't you just say in previous sentence that Asian Pb was not correlated with O3?

At UNRG, CO and NO_x increased during the morning commute (05:00 to 08:00 PST); O_3 started to increase at 07:00 and stayed elevated until 20:00(SI Fig. 2). The morning increase was due to local sources, and down mixing from the free troposphere, similar to what has been observed in valleys of Nevada, including Reno (Gustin et al., 2015b; Gustin et al., 2013) and in

California (Burley and Bytnerowicz, 2011). The same diel pattern was observed at UNRG in 2014 and 2015 (SI Fig. 2 and 3). This site is located <30 m from a highway, and the pattern of criteria pollutants at this location show an association with local mobile sources (SI Fig. 2 and SI Tables 12-15). During the 2014 sample period at UNRG, O_3 (daily average) was impacted by regional transport bringing air pollution from San Francisco, Sacramento, and the San Joaquin Valley up the I-80 corridor (CARB, 2001) and Yuba River gap, indicated by the short-term O_3 measurements (max 1 h, MDA8) being positively correlated with SO_2 and NO. O_3 (daily average, max 1 h, MDA8) was also impacted by long-range transport, indicated by positive correlations with N. Eurasia and E. Asia trajectories.

RM compounds at UNRG were primarily indicative of quick oxidation reactions associated with highway pollutants (nitrogen and sulfur compounds, Gustin et al., 2016); however, a mixture of compounds was observed, including halogenated compounds ($HgBr_2$ and $HgCl_2$). RM was negatively correlated with all trajectories from N. Eurasia and E. Asia, and with O_3 ($p<0.1$), max 1 h O_3, MDA8 O_3 (SI Table 12) indicating RM did not arrive with trans-Pacific air masses, but halogenated compounds suggest a marine boundary contribution and local and regional oxidants impacting concentrations. Both PEAV and UNRG had little influence from the Las Vegas source box.

For the days with Pb isotope data at UNRG (19 days, SI Tables 16-20), Pb measured at UNRG was also impacted by long-range transport from E. Asia. Pb isotopes measured at UNRG during this time were located on the California Array, again on a mixing line that had a different slope from PEAV (slope=1.04, $r^2 = 0.83$) and overlapped ores from Russia, Mongolia, and Kazakhstan toward the Asia array (Fig. 1a). UNRG and PEAV Pb days were analyzed for the same day at both sites due to the proximity of the two sites. UNRG had ~1.9 times the amount of Pb and ~1.5 times the amount of Asian Pb compared to PEAV, confirming that PEAV is more rural but may intercept long-range air masses. Additional Pb isotopic data from Eurasia (Fig. 1 grey data points from: Bollhöfer and Rosman, 2001; Bollhöfer and Rosman, 2002; Brown, 1962; Doe, 1970; Hopper and Ross, 1991) show that N. Eurasian sources need to be considered.

Figure 1: Plot of $^{206}Pb/^{207}Pb$ vs. $^{208}Pb/^{207}Pb$ for 2014 data at a) UNRG and PEAV 2014, and b) UNRG and GBNP 2015, including data from previous studies. Data from California is in blue, Asia in black, UNRG in yellow, PEAV in red, GBNP in green, and N. Eurasia in grey. Data include Mt. Tamalpais, Chabot science center, CA, central CA, Chinese Loess and Hefei, China

(Ewing et al., 2010), Eurasian aerosols (Bollhöfer and Rosman, 2001; Bollhöfer and Rosman, 2002), Chinese coal (Díaz-Somoano et al., 2009; Tan et al., 2006), Chinese Loess (Jones et al., 2000), Russian ores (Brown, 1962; Doe, 1970; Hopper and Ross, 1991), and Great Basin National Park, NV (Christensen et al., 2015). Red circle indicates anomalous data point.

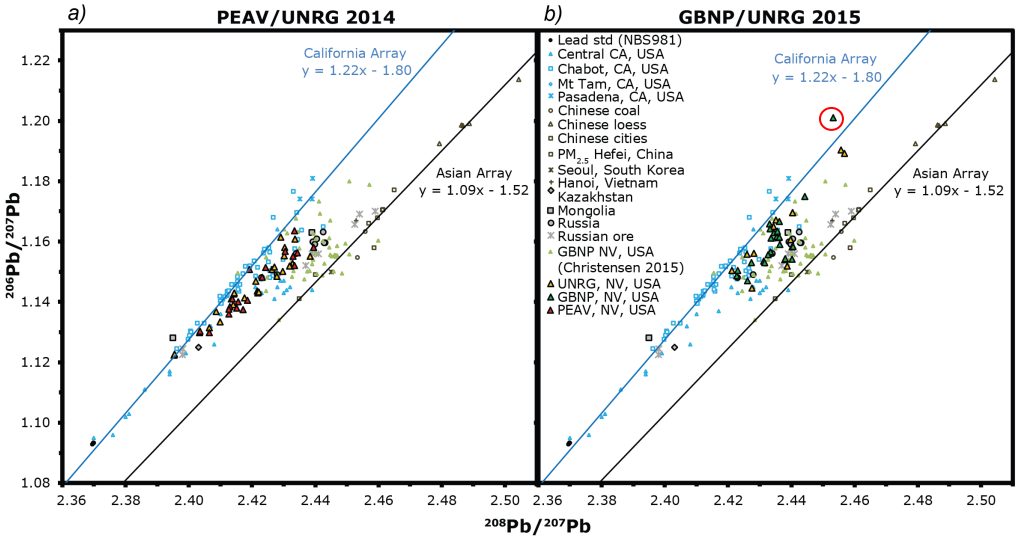

4.2 GBNP and UNRG 2015

The diel pattern at GPNP during spring and fall 2015 (SI Fig. 4), shows an increase in O_3 of ~6 ppbv starting at 05:00 to 11:00 PST that stayed elevated until 16:00 as air was mixed down to this high elevation location. When looking at the fine resolution data (SI Fig. 4b), nighttime CO (120 ppb) and NO_x (0.55 ppb) concentrations increased by 12 ppb and 0.6 ppb, respectively, at 06:00 PST, then declined and increased again mid-morning (10:00 PST), and then declines and increase again mid-afternoon (16:00 and 18:00 PST, respectively), suggesting local source impacts, also seen in previous work (Miller et al., 2015). Mean O_3 at GBNP during this period (48±9 ppbv) was also similar to previous studies (46±9 ppbv, Miller et al., 2015).

For this sample period at GBNP (SI Tables 21-24), O_3 (daily average, max 1 h, MDA8) was positively correlated with $PM_{2.5}$, CO, temperature, solar radiation, total and >3 km trajectories from N. Eurasia, >3 km trajectories from E. Asia, and >3 km trajectories from over San Francisco and negatively correlated with NO_x and RH. This indicates that GBNP O_3 was impacted by long-range transport, with some impact from regional and local sources. GBNP experiences differing conditions based on season (Fine et al., 2015a; Fine et al., 2015b; Gustin et

al., 2015b). Air masses often approach GBNP from the southwest in the spring, particularly during cyclonic flow that disrupts prevailing westerly wind patterns (Fine et al., 2015a; Fine et al., 2015b; VanCuren and Gustin, 2015), bringing regional pollution from Los Angeles and Las Vegas (SI Table 25). In summer, GBNP has more local tourist activity. Increased photochemical reactions, convective mixing in the summer also facilitates interception of trans-Pacific air masses, and a stronger positive correlations with long-range air masses (SI Table 26)

RM at GBNP (SI Table 21) was positively correlated with $PM_{2.5}$, O_3 (daily average, max 1 h, MDA8), temperature, solar radiation, and trajectories from Los Angeles and Las Vegas. RM was negatively correlated with NO_x, RH, and all trajectories from N. Eurasia and E. Asia. This indicates that regional sources were facilitating production of RM and that RM from Eurasia was lost due to deposition or conversion to GEM, this is also supported by the a negative correlation between % Asian Pb and RM (SI Table 24).

For the days with Pb isotope analysis at GBNP (22 days, SI Tables 27-31), total Pb mass and total Asian Pb mass were positively correlated with O_3. Percent Asian Pb was positively correlated with total and >3 km trajectories from E. Asia, and negatively correlated with <1 km trajectories from Los Angeles and <1 km ($p<0.1$) trajectories from Las Vegas, indicating the importance of Asian sources of Pb to GBNP. Pb isotopes measured at GBNP during this time were located on the California Array and on a mixing line that had a slope of 0.79 ($r^2 = 0.44$, Fig. 1b)

For this sample period, at UNRG (SI Tables 32-35), significant positive correlations between O_3 and ABLH, N. Eurasia and E. Asia indicated that daily average, max 1 h, MDA8 O_3 at UNRG during this period were influenced by long-range transport (SI Table 35). $PM_{2.5}$ was positively correlated with other pollutants (RM, CO, NOx, and NO), highlighting the urban nature of this site.

RM at UNRG during this period (SI Table 32) was positively correlated with $PM_{2.5}$, solar radiation, temperature, and <1 km trajectories from San Francisco. RM was negatively correlated with O_3 (daily average, max 1 h, MDA8), and all trajectories from N. Eurasia, and from E. Asia. Again, indicating local and regional impacts were greater than long-range impacts, supported by nitrogen and sulfur based RM compounds measured during this time (Gustin et al., 2016).

For days with Pb isotope analysis at UNRG (11 days, SI Tables 36-40), daily average O_3, max 1 h O_3 ($p<0.1$), and MDA8 O_3 were positively correlated with % Asian Pb. Filters analyzed for Pb were biased towards understanding O_3 events (noted below), so this correlation makes sense.

At UNRG during this time, total Pb mass was greater, total Asian Pb mass was higher, and the % Asian Pb was similar to that measured at GBNP. It is important to note the differences in samples between UNRG (n=11) and GBNP (n=23). Pb isotope ratios for UNRG lie between the Asia and California arrays on a mixing line that had a slope of 1.17 ($r^2 = 0.77$), and indicate a Eurasian influence (Fig. 1b). There is one anomalous point from GBNP on September 3, 2015 with -28% Asian Pb (circled in red in Fig. 1b), which may be due to an issue with the Pb extraction process, but is unclear. Trajectories for this time (SI Fig. 5) remain over the Pacific Ocean, southern California, and western Mexico, with minor transport from N. Eurasia and central USA. It is uncommon to have trajectories in this area track over central USA, which could explain the anomalous data; however, HYSPLIT only indicates two trajectories out of 216 from this area. Two days at UNRG during the same time (August 31 and September 2) had similar high 208/207 Pb ratios but lower 206/207 Pb ratios. The September 3, 2015 data point was not included in the Pearson correlation analyses or in the linear fit in the data but is included in Table 2 and Fig 1b.

John Christensen 8/18/17 9:52 AM

Comment: I can't think of a lab issue that would cause this. Was it a particularly small sample? or had larger than usual errors? It is odd, though there are a few other data points to the left of the Calif array, and you might leave it at that.

5. Discussion:

5.1 Case studies

Complex weather dynamics affect the transport of atmospheric pollutants in the Western USA. To understand this phenomenon, specific events were assessed as case studies. These case studies were selected based on % Asian Pb, concentrations of O_3 (daily average, max 1 h, MDA8), RM, CO, and RH values. Days were selected when these values were above the monthly median (RH below monthly median), indicating pollution transport events and compared to days below the monthly median.

5.1.1 June 2014

Pb samples were analyzed for June 6, 12, and 17, 2014 at PEAV and UNRG (SI Fig. 6). During this time, weather maps indicated a low-pressure system at the surface (SI Fig. 7a-d) and cyclonic flow at 500 mb moved from W to E across the top of Nevada (SI Fig. 8a-d), while a cold front associated with the low moved W to E across Nevada. Pressure measured at PEAV dropped across this period and temperature decreased (16, 12, and 3° C on the 3 days). ABLH measured at 16:00 PST lowered from 3.2 to 1.9 km, and then returned to 3.5 km. Wind speed at PEAV and UNRG was higher on June 12 at 16 m s^{-1} and 3.7 m s^{-1} compared to median monthly values of 3.1 m s^{-1} and 2.0 m s^{-1}, respectively. RH was lower than the monthly median on June 6 and 12 at both PEAV and UNRG and higher than the monthly median on June 17 (SI Fig. 9 and 10). Influence from the total E. Asia trajectory box on these days, decreased from 1.0% to 0.019%, and then increased to 0.15%. At the same time, influence from N. Eurasia decreased and increased 5.0%, 1.8%, and 16%. Trajectories for June 12 (Fig. 2a and 3b) resided mainly over the Pacific Ocean. On June 9 and 10 at PEAV, there was an increase in $PM_{2.5}$, O_3 (daily average, max 1 h, MDA8), RM, CO, and influence from N. Eurasia and E. Asia trajectories. Influence from N. Eurasia remained elevated through June. It is likely that air masses being transported over the Pacific Ocean at this time were polluted and the low-pressure system and associated cold front brought this air to the surface along with air from the San Francisco area.

On June 12, percent Asian Pb was 41%, higher than the 75th percentile (36%) at PEAV. At PEAV $PM_{2.5}$, O_3 (daily average, max 1 h, MDA8), and RM increased on June 12 above the monthly medians for each measurement. During this period, RM compounds differed slightly between the two sites with HgO, $HgCl_2$, and $HgBr_2$ seen at PEAV, and $HgCl_2$ and $HgBr_2$ at UNRG (Gustin et al., 2016). RM compounds appear to be influenced by interaction with the MBL. CO at PEAV was below the monthly median for all 3 days as the front moved through (SI Fig. 9b). On June 12 at UNRG, percent Asian Pb was 47%, higher than the 75th percentile (42%) for Pb samples at UNRG in 2014. $PM_{2.5}$, WCAQ O_3 (daily average, max 1 h, MDA8), and RM increased on June 12 above the monthly medians for each measurement. CO was above the monthly median for June 6 and 12, and below on June 17 (SI Fig. 10b). This is an example of input of Trans-Pacific pollution associated with frontal activity as described by Knowland et al. and VanCuren et al. (2015; 2005). June 2014, both PEAV and UNRG had halogenated RM compounds and elevated influence from >3 km trajectories from over San Francisco. June 2014,

MDA8 O_3 was enhanced by 2-7 ppbv above the monthly median at GBNP and 4-9 ppbv at UNRG.

Figure 2a and b: HYSPLIT 10-day back trajectories for a) PEAV and b) UNRG June 12, 2014. Trajectory points are colored by altitude height (m agl). FRP points are sized based on power (MW), white circles indicate the most recent day back, light grey circles indicate an intermediate day back, and grey circles indicate the furthest day back. Black boxes indicate the five source boxes.

a)

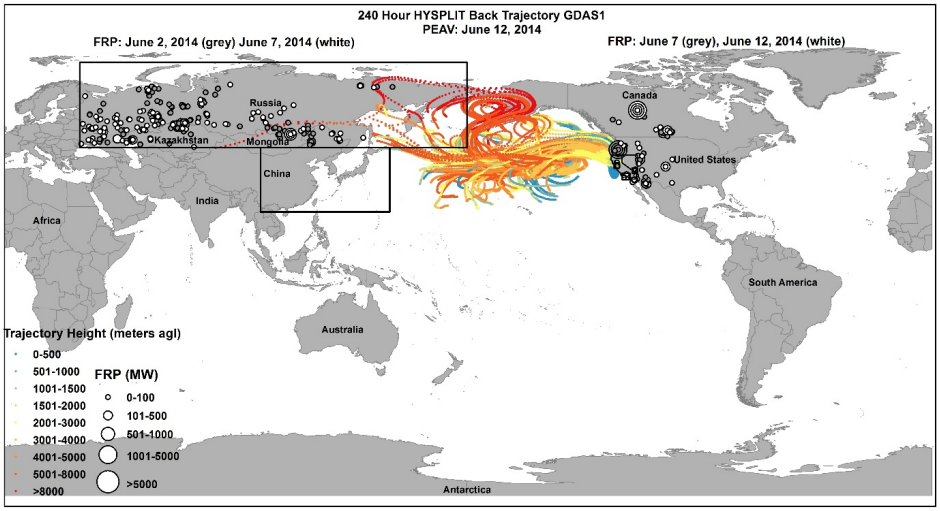

b)

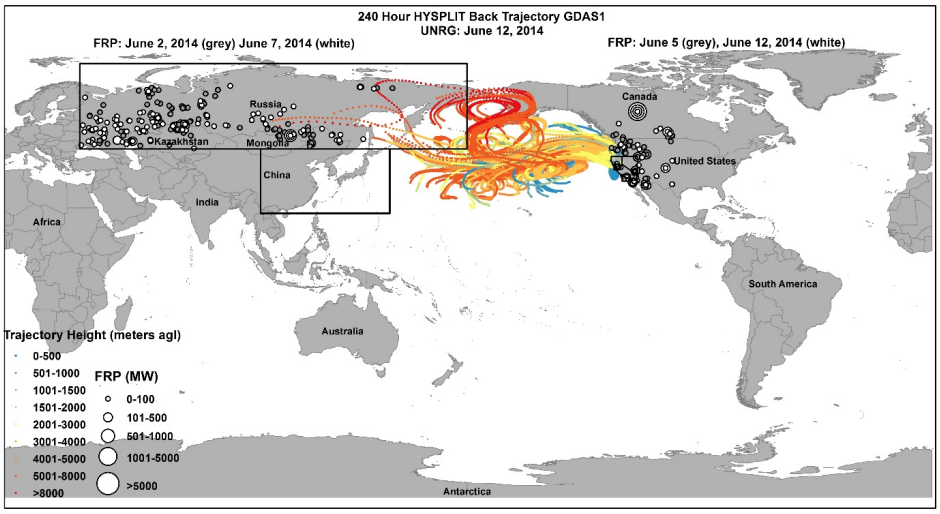

564
565

566 5.1.2 September/October 2014

567 From September 13 to October 31, 2014, the King Fire burned over 390 km^2 in
568 California, southwest of Reno, NV (CA, 2017). On September 22 and 24, $PM_{2.5}$, O_3, CO were all
569 above monthly medians (SI Fig. 11 and 12) at PEAV and at UNRG on September 22 due to
570 influence from this fire, seen in SI Fig. 13 from the Naval Research Laboratory Aerosol Analysis
571 and Prediction System (NAAPS, https://www.nrlmry.navy.mil/aerosol/). RH on September 22
572 was higher than the monthly median at PEAV and UNRG due to emission of water vapor
573 associated with biomass burning , (SI Fig. 11a & 12a,Parmar et al., 2008). RM at both sites was
574 lower than the monthly median. RM compounds at the end of September were not discernible at
575 PEAV. At this time, UNRG had nitrogen and sulfur RM compounds (Gustin et al., 2016).
576 Influence from local (King fire) and regional sources dominated this period.Pevious large fires
577 west of Nevada have also impacted air quality in Nevada (Rim Fire 2013, Miller et al., 2015).
578 On September 27, October 15, and 17, Pb samples at PEAV were greater than 36% Asian
579 Pb (SI Fig. 14). September 27, October 9, and October 17 Pb samples at UNRG were greater
580 than or equal to 42% (SI Fig. 14). Although September 27 had high percent Asian Pb (58% at
581 PEAV and 42% at UNRG), there was moderate input of air from N. Eurasia and San Francisco,
582 which may reflect previously deposited Asian Pb being re-mobilized during the fire and mixed
583 with local and regional sources. Precipitation was observed that day, likely lowering pollutant

concentrations; $PM_{2.5}$, O_3, CO, and RM were all below monthly medians. RM compounds were different during the end of September and start of October, PEAV had $HgCl_2$, $HgBr_2$, and nitrogen compounds indicating input from the marine boundary layer, while UNRG had nitrogen and sulfur RM species (Gustin et al., 2016). October 15 and 17 at PEAV had $PM_{2.5}$, above the monthly median and RM below the monthly median. October 17 had O_3 (daily average, max 1 h, MDA8) and CO concentrations higher than the monthly medians (there were no CO measurements for October 15). Temperature on October 17 was higher, while wind speed was lower than October 15. N. Eurasia and E. Asia TRTs doubled from October 15 to October 17 (Fig. 3a and b). A low-pressure system and cold front moved through the area between October 15 and 17 (SI Fig. 15), bringing down drier air from the free troposphere and stratosphere, demonstrating that trans-Pacific air masses can influence the Western USA in the fall. In September 2014, MDA O_3 was initially suppressed 12 ppbv during heavy fire impacts and then enhanced 18 ppbv as the fire plume aged. In October, PEAV MDA O_3 was enhanced 5-7 ppbv, while UNRG saw little enhancement during this time.

Figure 3a and b: HYSPLIT 10-day back trajectories for a) PEAV and b) UNRG October 17, 2014. Trajectory points are colored by altitude height (m agl). FRP points are sized based on power (MW), white circles indicate the most recent day back, light grey circles indicate an intermediate day back, and grey circles indicate the furthest day back. Black boxes indicate the five source boxes.

a)

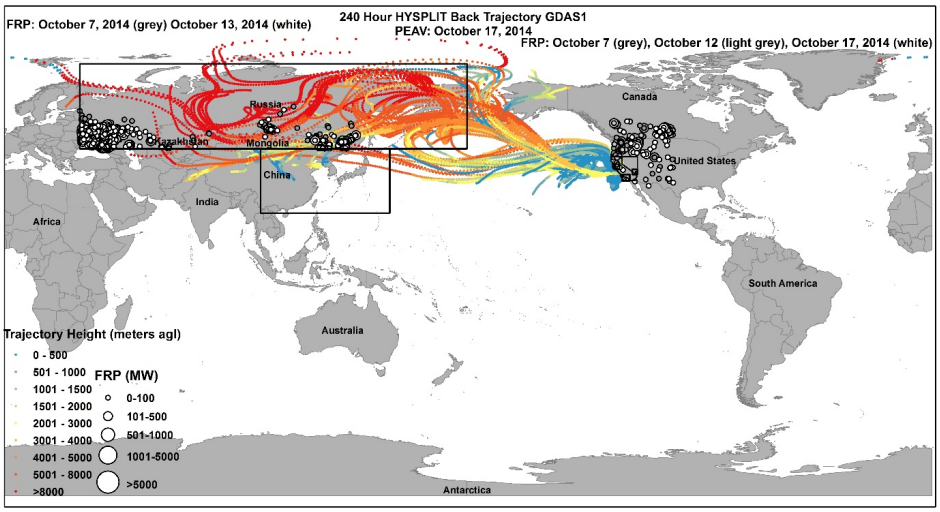

b)

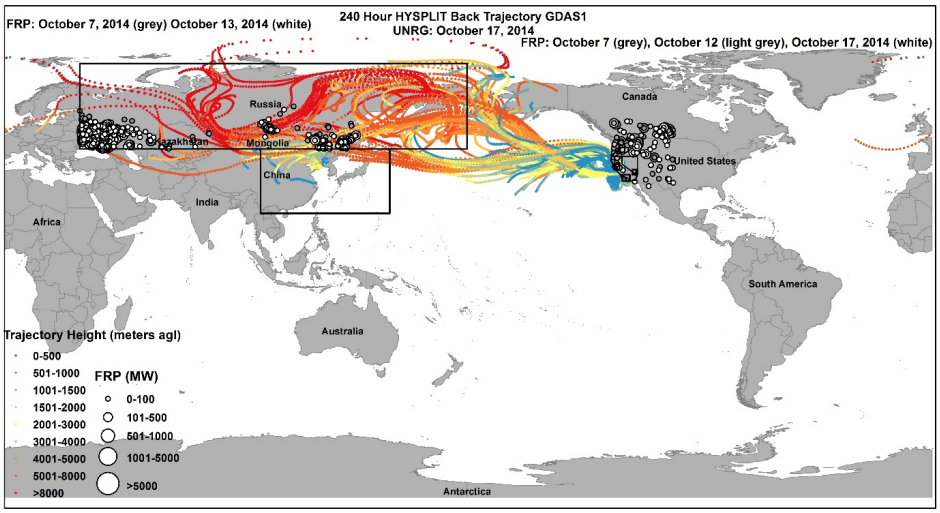

5.1.3 March 2015

Two low-pressure systems moved NW to SE and an associated cold front moved across the state from March 28 to 29, and March 31 to April 1 (SI Fig. 16). There were no CO or NO_x measurements for this period at GBNP. March 27 at GBNP had lower $PM_{2.5}$, O_3 (daily average, max 1 h, MDA8), and RM than monthly medians and RH only slightly lower than the monthly median. March 31 had higher $PM_{2.5}$, O_3 (daily average, max 1 h, MDA8), and RM than the monthly median and RH was half of the monthly median (SI Fig. 17). On March 31, there was influence from the E. Asia source box greater than the 75th percentile for the site and three times March 27, which doubled the next day as the low continued to move through. There was also influence from the San Francisco source box above the 75th percentile on March 31. March 31 had the highest Pb mass (0.70 ng m^{-3}) of the 22 days analyzed for Pb, but was only 38% Asian Pb compared to March 27 (0.15 ng m^{-3}), which was 65% Asian Pb (SI Fig. 18). As the low-pressure system moved west to east, GBNP saw an increase in trans-Pacific, Los Angeles, and Las Vegas trajectory influence while UNRG saw increases in trans-Pacific and >3 km trajectories from over San Francisco.

UNRG had a similar pattern for March 28 and March 31 for $PM_{2.5}$ and CO. O_3 (daily average, max 1 h, MDA8) for both days was higher than the monthly median (SI Fig. 19). RH

was lower than the monthly median for both days. RM was higher than the monthly median on March 31. Influence from N. Eurasia and E. Asia were both higher than the 75th percentile for this period, there was some influence from San Francisco as well.

The HYSPLIT back trajectories for March 27 from GBNP and March 28 from UNRG (Fig. 4a and 5b) show minimal trajectories through E. Asia and most of the trajectories stayed low above the Pacific Ocean. The NAAPS optical depth maps (SI Fig. 20) show a plume with moderately high optical depth moving from W to E across the Pacific towards Western North America, March 30 to March 31, 2015. HYSPLIT back trajectories for March 31 at GBNP and UNRG (Fig. 4c and 5d) show air masses moving very quickly, several of which made it around from Greenland and Eastern North America. Trajectories coming into GBNP stayed mostly south of the N. Eurasian source box in the E. Asian source box while trajectories coming into UNRG had a mix of E. Asia and N. Eurasian influence. Percent Asian Pb was lower on March 31 due to the combination of local sources and long-range transport from Eurasia as well as the eastern US.

MODIS FRP (Fig. 4c and 5d) shows multiple large fires in the N. Eurasia source box and east of Nevada, occurring during this time. IMPROVE data (SI Fig. 21) for March 31 at GBNP shows elevated potassium (K) over the monthly mean, a tracer for biomass burning, as well as aluminum (Al), chloride (Cl-), chlorine (Cl), iron (Fe), magnesium (Mg), sea salt, silicon (Si), sodium (Na), and soil. Although March 31 was influenced by trans-Pacific air, the fast moving air likely picked up many sources of pollution including local and regional (SI Fig. 22), contributing to O_3 concentrations at GBNP and UNRG (67 and 69 ppbv, respectively) approaching the NAAQS concentration for the design value. MDA8 O_3 was enhanced by 2-16 ppbv above the monthly median at GBNP and 5-14 ppbv at UNRG during these events.

Figure 4a, b, c, and d: HYSPLIT 10-day back trajectories for GBNP March 27 (a), 31 (c) and UNRG March 28 (b), 31 (d), 2015. Trajectory points are colored by altitude height (m agl). FRP points are sized based on power (MW), white circles indicate the most recent day back, light grey circles indicate an intermediate day back, and grey circles indicate the furthest day back. Black boxes indicate the five source boxes.

a)

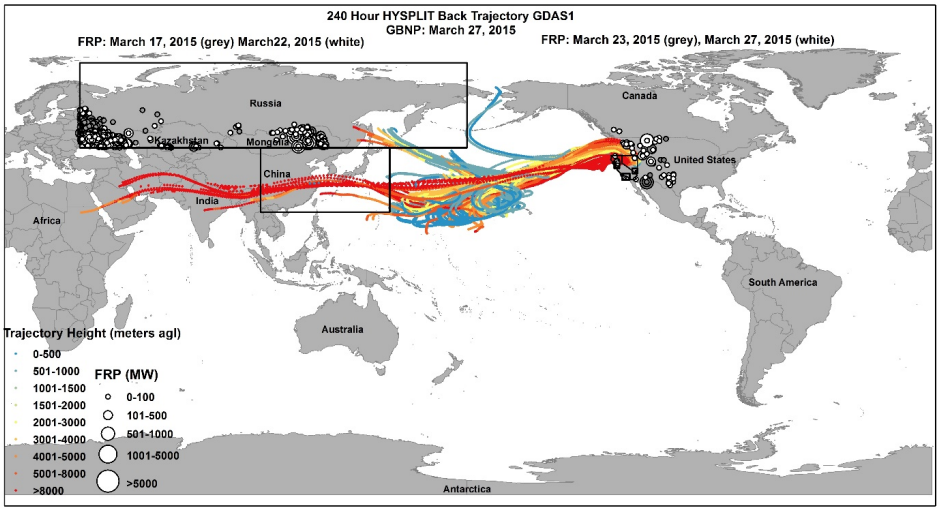

657
658 *b)*

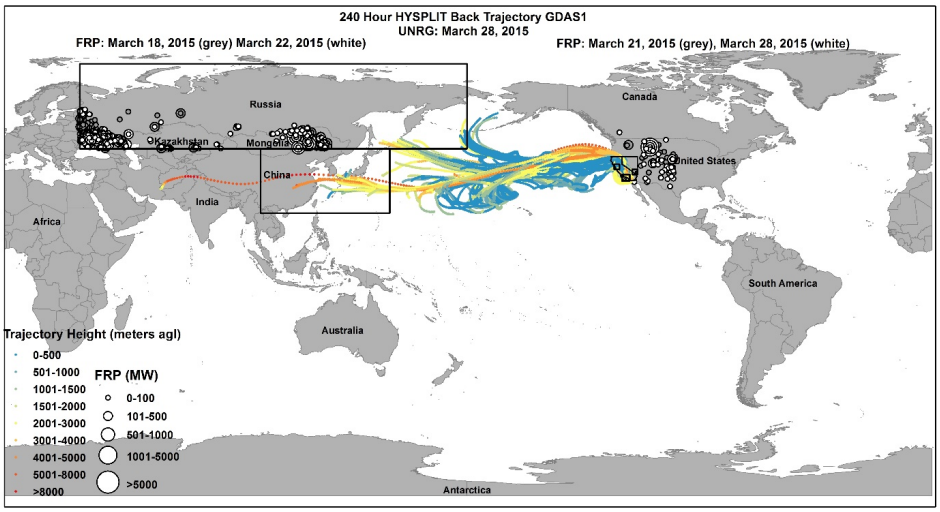

659
660 *c)*

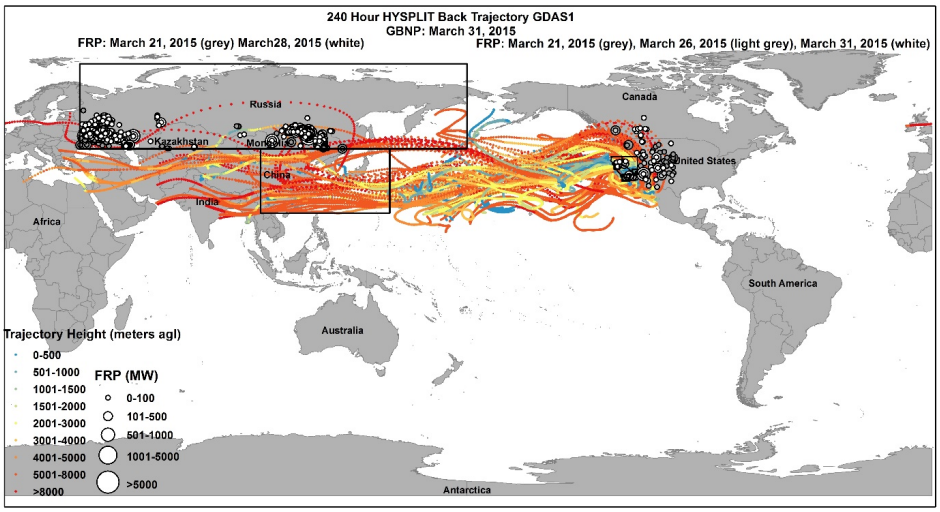

d)

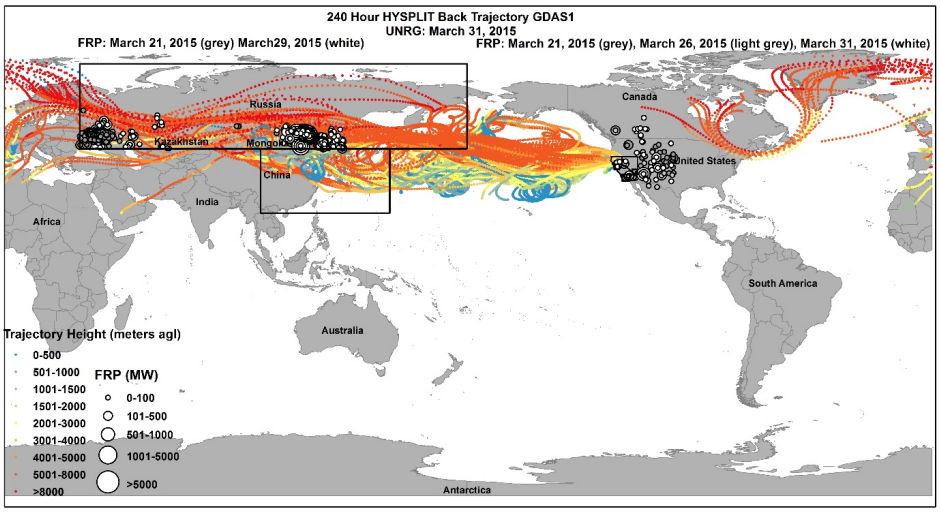

5.1.4 June 2015

June had the highest mean monthly O_3 (56 ppbv daily, 65 ppbv max 1 h, 62 ppbv MDA8) concentrations of the six-month study period at GBNP. Eight days in June were analyzed for Pb isotopes (SI Fig. 23). On June 8 and 9 at GBNP MDA8 was above the 70 ppbv concentration used for the NAAQS, decreasing from June 8 to June 9. CO, NO_x, and NO were all above the monthly median. $PM_{2.5}$ was below the monthly median but decreased on June 9 further, RM also

671 decreased. RH dropped from 38% on June 8 to 29% on June 9; both days were below the
672 monthly median (SI Fig. 24), there was a small amount of precipitation on June 8. Influence
673 from the N. Eurasia and E. Asia source boxes decreased by half, both below the 75th percentile.
674 There was no influence from the <1 km San Francisco box and minimal influence from the <1
675 km Los Angeles and Las Vegas boxes, air mainly arrived >3 km over these source boxes (Fig. 5a
676 and b). From June 8 to June 9, a high-pressure area stagnated over Nevada and the rest of the
677 inland Western USA, while low pressure occurred over California and a weak cyclonic system
678 remained at the 500 mb level over Nevada (SI Fig. 25 and 26), bringing air aloft down to the
679 surface. Speciated $PM_{2.5}$ IMPROVE data (SI Fig. 27) had elevated sulfate (SO_4, NH_4SO_4), Si,
680 and sulfur (S) on June 8, generally considered tracers of long-range transport of pollutants
681 associated with combustion from Asia (Christensen et al., 2015). Total Pb mass decreased
682 slightly, but percent Asian Pb stayed the same (61%) for both days.
683 At UNRG, as the high-pressure system remained over Nevada ($PM_{2.5}$, O_3 daily average,
684 max 1 h O_3, MDA8 O_3, and CO), pollutant concentrations increased from June 8 to June 9 (SI
685 Fig. 28). NO_x decreased and RH increased with some precipitation. Solar radiation decreased,
686 wind speed and temperature were similar. RM concentrations did not change between the two
687 days. Influence from N. Eurasia and E. Asia decreased over the two days at similar magnitudes
688 as the TRTs for GBNP. Influence from San Francisco trajectories slightly increased. Trajectories
689 from Las Vegas and Los Angeles were similar for the two days (~1.1% and 0.03%, respectively),
690 both were higher than the 75th percentile for the sample period (~0.03% and 0.0%, respectively).
691 Total Pb mass increased and percent Asian Pb went from 40% to 74% between the two days.
692 During this period, it is likely the Western USA was influenced by long-range transport and
693 possibly STE as air aloft subsided.
694 At GBNP, on June 17 and 18, max 1 h O_3 was over 70 pbb and MDA8 O_3 was 67 and 68
695 ppbv respectively, all higher than the monthly medians. $PM_{2.5}$ on June 17 was slightly higher
696 than the monthly median and dropped below on June 18. CO, NO_x, and NO increased across the
697 two days, NO_x on the second day and NO on both days were above the monthly medians. RH
698 was below the monthly median on both days. Influence from >3 km trajectories over the N.
699 Eurasia source box dropped by half over the two days but were ~3 and 2 times higher than the
700 75th percentile value (Fig. 5c). Influence from <1 km from San Francisco decreased over the two
701 days but was higher than the 75th percentile on both. Trajectories <1 km from Los Angeles and

Las Vegas decreased but were below the 75th percentile. Total Pb mass was similar on the two days as was % Asian Pb (~40%). There was a high-pressure system that moved across the state, June 16 to 17, and lows surrounding the state. Cyclonic flow at the 500 mb pressure height remained over the state on June 17 and 18 (SI Fig. 29 and 30). IMPROVE data (SI Fig. 31) from June 17 had elevated Al, nitrates (NH_4NO_3, NO_3), sulfates (NH_4SO_4, SO_4), calcium (Ca), Cl-, Fe, Mg, sea salt, Si, and soil, above the monthly mean, pointing to local and long-range pollution sources. During this period, it is likely the Western USA was influenced by long-range transport and possibly STE as air aloft subsided as well as regional pollutants from Los Angeles and Las Vegas (SI Fig. 24c and 28c). The trajectory residences times clearly illustrate trans-Pacific air masses peaking at UNRG ~2 days before peaking at GBNP (SI Fig. 24c and 28c) as the high-pressure system moved across the state. In June 2015, MDA8 O_3 was enhanced by 4-10 ppbv above the monthly median at GBNP, and 7-9 ppbv at UNRG.

Figure 5: HYSPLIT 10-day back trajectories for (a) GBNP June 9, (b) UNRG June 9, and (c) GBNP June 17, 2015. Trajectory points are colored by altitude height (m agl). FRP points are sized based on power (MW), white circles indicate the most recent day back, light grey circles indicate an intermediate day back, and grey circles indicate the furthest day back. Black boxes indicate the five source boxes.

a)

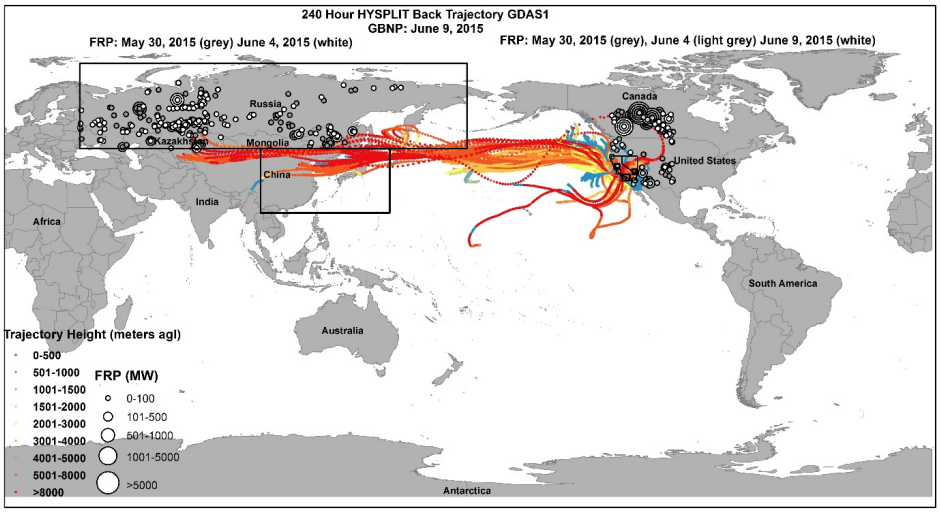

b)

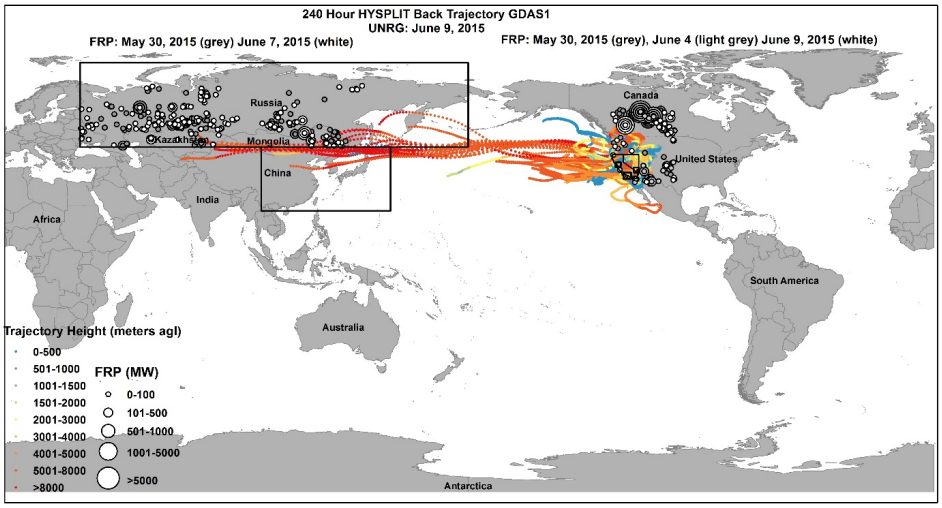

c)

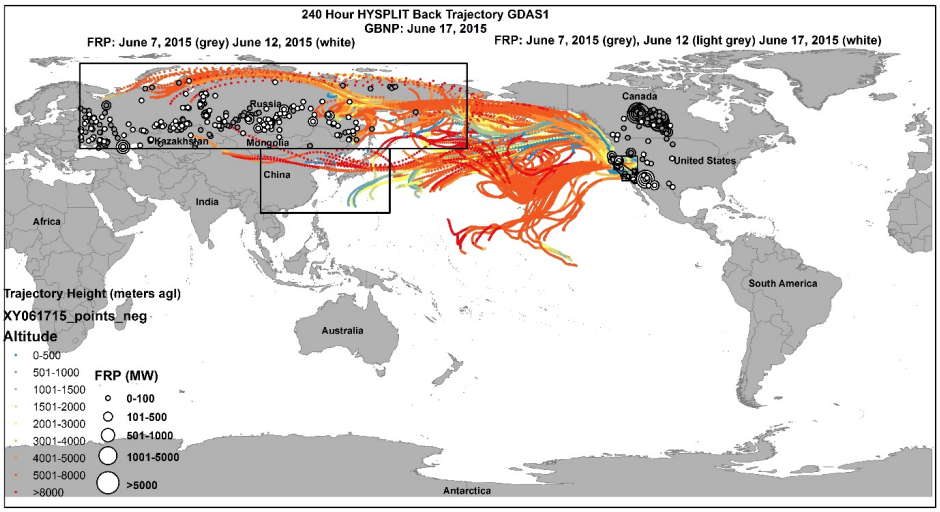

5.1.5 September 2015

On September 10, 2015 at GBNP, $PM_{2.5}$, O_3 (daily average, max 1 h, MDA8), CO, RM were all elevated above the monthly medians (SI Fig. 32). RH was below the monthly median. N. Eurasia trajectories were above the 75th percentile. TRT from the E. Asia source box decreased from the previous two days; however, percent Asian Pb was 74% (SI Fig. 32c and 33). TRTs from San Francisco were greater than the 75th percentile while trajectories from Los

Angeles and Las Vegas (<1 km) were zero (SI Fig. 32c). FRP data show several fires in the trajectory paths with high FRP in the N. Eurasia source box and large FRP values in California (Fig. 6). Trajectories also arrived from over Canada and Alaska.

Surface weather maps show a high (SI Fig. 34) over Nevada and a weak cyclonic flow at the 500 mb level (SI Fig. 35); indicating that air aloft was mixed down to the ground. Before the high-pressure formed, Los Angeles trajectories had a strong influence on GBNP, which decreased with the high-pressure system (SI Fig. 32c). IMPROVE data (SI Fig. 36) shows elevated organic mass (OMC), due to local smoke (SI Fig. 37). Although O_3 concentrations were not approaching the NAAQS concentration on this day, concentrations were elevated above the monthly medians(SI Fig. 32), again demonstrating that long-range transport of air masses can influence pollutants in the Western USA outside of the spring months. Local sources, such as wildfires, may complicate the signature of long-range transport. In September 2015, MDA O_3 was enhanced by 17 ppbv above monthly medians at GBNP, with little enhancement at UNRG (SI Fig. 38).

Figure 6: HYSPLIT 10-day back trajectories for GBNP September 10, 2015. Trajectory points are colored by altitude height (m agl). FRP points are sized based on power (MW), white circles indicate the most recent day back, light grey circles indicate an intermediate day back, and grey circles indicate the furthest day back. Black boxes indicate the five source boxes.

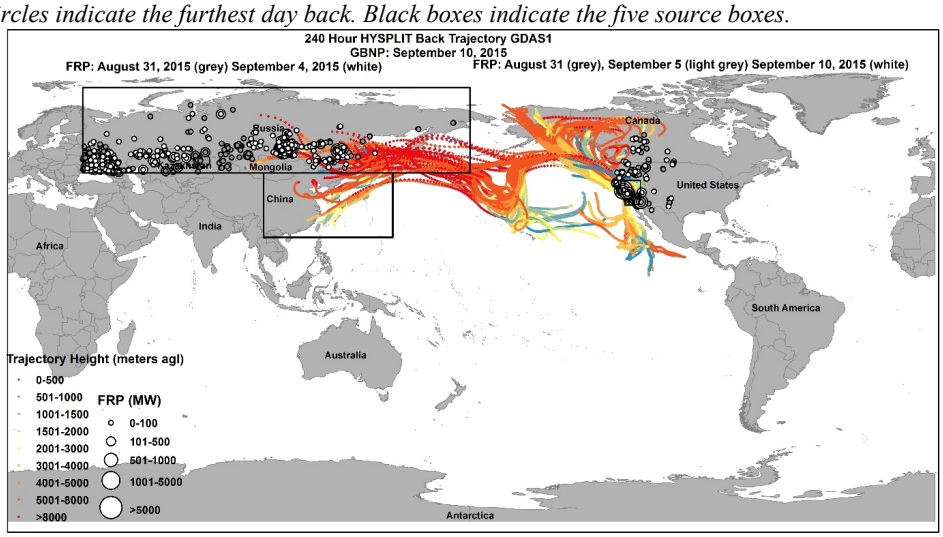

6. Conclusions:

Diel patterns of O_3 at the two high elevation sites had smaller ranges (<10 ppbv) and elevated O_3 compared to the lower elevation, urban site (>30 ppbv) similar to previous studies (Fine et al., 2015a). At both high elevation sites, max 1 h O_3 was positively correlated with $PM_{2.5}$ and CO, indicative of transport of pollutants from regional and long-range sources. Lower concentrations of $PM_{2.5}$ and CO at the two high elevation sites illustrated the rural nature compared to UNRG. Ozone was positively correlated with RM at both sites while RM was negatively correlated with RH, similar to free tropospheric data from Weiss-Penzias et al. (2015), indicating formation of RM from photo-oxidation of GEM in dry upper altitude air. Total Pb mass, total Asian Pb mass, and % Asian Pb were generally positively correlated with trajectories from E. Asia. GBNP air was influenced by Las Vegas and Los Angeles during the sample period, while western Nevada sites were not.

UNRG had different conditions between the sample year (2014 versus 2015), and from the two high elevation sites. Ozone (daily average, max 1 h, MDA8) was negatively correlated with RM for both sample periods at UNRG. This may be due to rapid deposition of HgO, created as O_3 increased, reducing measured RM. RM at UNRG was generally negatively correlated with N. Eurasia and E. Asia trajectories and positively correlated with >3 km (2014) and <1 km (2015) trajectories from San Francisco. RM measurements consisted of nitrogen- and sulfur-based compounds with periodic halogen species, indicating influence from regional sources and the MBL. At UNRG in 2014 (summer and fall), total Pb mass, total Asian Pb mass, and % Asian Pb were positively correlated with trajectories from E. Asia; however, this was not the case in 2015 (spring-summer-fall) sample period, possibly due to the difference in sample period. Differences in RM compounds at PEAV and UNRG further support that the high elevation site differs from the urban, lower elevation site and that air quality can differ between two sites located close together (~12 km) due to differences in transport between a valley and a high elevation site.

The case studies demonstrated that in a 240 h back trajectory period, air masses can originate in E. Asia as well as from other parts of Eurasia and eastern North America. Trans-Pacific air masses not only influenced the Western USA in spring, but also in the fall (September 2014 and 2015). Ozone was often elevated following passage of low-pressure systems and associated cold front also seen in Knowland et al. (2015) and Lin et al. (2012) and when there was a high-pressure system at the surface and cyclonic flow aloft, bringing O_3 down to the

surface seen in Cooper et al. (2011). Increased trans-Pacific air masses contributed to elevated O_3 above monthly medians. The ubiquitous influence of Eurasian Pb and positive correlations between Pb mass and O_3 at the two high elevation sites indicates long-range transport of pollutants. During pollution events, long-range transport not only affects baseline concentrations, but can also be the primary reason for increased concentrations associated with discrete pollution plumes traveling in the free troposphere that may or may not be delivered to the surface in Nevada (Fine et al., 2015b; Langford et al., 2015b).

In spring (end of March 2015), low-pressure systems moved west to east with associated cold fronts impacting measurements at GBNP and UNRG, marked by a decrease in RH and increases in RM, O_3, and $PM_{2.5}$ concentrations all above monthly medians. Increased frontal activity in the Western USA facilitated entrainment of drier air aloft combined with increasing temperatures and photochemical reactions. In summer, higher overall concentrations of O_3 occurred in both years. In June 2014 there was frontal activity causing entrainment, while June 2015 was characterized by high-pressure systems in the area causing subsidence of air bringing pollutants aloft to the surface. In fall, September/October 2014, a low-pressure system and cold front also moved through the area, bringing down drier air from the free troposphere and stratosphere, demonstrating that trans-Pacific air masses can influence the Western USA in the fall. In September 2015, there was a high over Nevada and a weak cyclonic flow at the 500 mb level; indicating that air aloft was mixed down to the ground, supported by the large influence of >3 km trajectories from over San Francisco at UNRG.

Fiore et al. (2014) modeled baseline O_3 (no recent local emissions, but includes aged domestic emissions) and North American Background (NAB, model constructed with zero North America emissions) MDA8 O_3 for a typical year at high elevation intermountain western sites (>1.5 km). Baseline was modeled at 60 ± 7 while NAB was 48 ± 8 using the GFDL AM3 model and 54 ± 6 and 42 ± 5 respectively for the GEOS-Chem model. These modeled baseline and background numbers agree well with other observational and modeling studies (Baylon et al., 2016; Cooper et al., 2011; Fiore et al., 2003; Lin et al., 2012; Zhang et al., 2011). Asian enhancement events to surface observations and models can contribute 8 to 15 ppbv at high-elevation sites in the Western USA when MDA8 O_3 exceeds 60 ppbv (Lin et al., 2012). Observed enhancements during strong trans-Pacific events, such as in March 2015, agree with this enhancement range.

Negative correlations between RM and % Asian Pb, N. Eurasia trajectories, and E. Asia trajectories suggests RM was removed from these air masses before reaching the sample sites due to deposition or conversion to GEM as suggested by Weiss-Penzias et al. (2015). RM at GBNP was also positively correlated with trajectories from Los Angeles and Las Vegas, indicating that regional oxidant sources facilitated production of RM. Reinemann et al. (2014), using sediment cores, also found that lakes in the Great Basin area were influenced by regional sources of Hg. Ozone at GBNP has also previously been shown to correlate better with southern Nevada sites (Fine et al., 2015a).

Monitoring sites are typically concentrated in urban centers or sensitive natural environments, leaving significant data gaps in rural areas, such as much of Nevada. This gap in data leads to poor understanding of air pollution sources influencing a region. Long-term monitoring sites with regular measurements are necessary for quantifying international atmospheric inputs that affect national standards and goals for international conventions. The TAPI Beta^{Plus} particulate measurement system may be too elaborate for long-term measurements at higher spatial density; however, it is useful for targeted experiments. Filter measurements are useful, low-cost methods for making multiple measurements ($PM_{2.5}$, RM, and Pb isotopes) simultaneously. Better understanding of the global cycling of pollutants will affect national and global policies, as standards to protect human and ecosystem health become more stringent, it will be necessary to understand the sources and processes influencing production and transport of atmospheric pollutants, particularly in areas far from sources, located in complex terrain, such as the Western USA.

Acknowledgments:

We acknowledge the Nevada Division of Environmental Protection (NDEP), the UNR College of Biotechnology and Natural Resources, and a USDA-HATCH grant for supporting this project. Thank you to Teledyne Advance Pollution Instrumentation (TAPI) for their collaboration on the TAPI Beta^{Plus} particulate measurement system setup and technical support. The FRP data used in this study is freely available from NASA. Balloon sounding data is available from Atmospheric Soundings Wyoming Weather Web, and the authors thank the site managers. Thank you to Dr. Rebekka Fine for initial research on the TAPI Beta^{Plus} particulate measurement systems for use in this project; to Matthieu Miller for site support, data collection,

and processing; to Dave Metts for allowing access to and support at the Peavine Peak site; to Kristien King for assistance with data processing; to Shaun Brown at LBNL for assistance; and to Christopher and Suzanne Pierce for support during sample analysis at LBNL. Support for the Center for Isotope Geochemistry at LBNL is provided by the Department of Energy, Office of Basic Energy Sciences through contract DE-AC02-05CH11231 to LBNL.

References:

AMAP/UNEP. Global Mercury Modelling: Update of Modelling Results in the Global Mercury Assessment 2013. Arctic Monitoring and Assessment Programme, Oslo, Norway/UNEP Chemicals Branch, Geneva, Switzerland, 2015.

Ambrose JL, Reidmiller DR, Jaffe DA. Causes of high O3 in the lower free troposphere over the Pacific Northwest as observed at the Mt. Bachelor Observatory. Atmospheric Environment 2011; 45: 5302-5315.

Baylon PM, Jaffe DA, Pierce RB, Gustin MS. Interannual Variability in Baseline Ozone and Its Relationship to Surface Ozone in the Western U.S. Environmental Science & Technology 2016; 50: 2994-3001.

Bertschi IT, Jaffe DA. Long-range transport of ozone, carbon monoxide, and aerosols to the NE Pacific troposphere during the summer of 2003: Observations of smoke plumes from Asian boreal fires. Journal of Geophysical Research: Atmospheres 2005; 110: n/a-n/a.

Bollhöfer A, Rosman KJR. Isotopic source signatures for atmospheric lead: the Northern Hemisphere. Geochimica et Cosmochimica Acta 2001; 65: 1727-1740.

Bollhöfer A, Rosman KJR. The temporal stability in lead isotopic signatures at selected sites in the Southern and Northern Hemispheres. Geochimica et Cosmochimica Acta 2002; 66: 1375-1386.

Brodin M, Helmig D, Oltmans S. Seasonal ozone behavior along an elevation gradient in the Colorado Front Range Mountains. Atmospheric Environment 2010; 44: 5305-5315.

Brown JS. Ore leads and isotopes. Economic Geology 1962; 57: 673.

Burley JD, Bytnerowicz A. Surface ozone in the White Mountains of California. Atmospheric Environment 2011; 45: 4591-4602.

CA SoCG. 2014 Large Fires List. In: Fire C, editor. Incident Information. 2017, 2017.

CARB CARB. Ozone Transport Assessment 2001. 2017, 2001.

Christensen JN, Weiss-Penzias P, Fine R, McDade CE, Trzepla K, Brown ST, et al. Unraveling the sources of ground level ozone in the Intermountain Western United States using Pb isotopes. Science of The Total Environment 2015; 530–531: 519-525.

Cooper O, R., Parrish D, D., Stohl A, Trainer M, Nedelec P, Thouret VC, J. P. Oltmans, S. J. Johnson, B. J. Tarasick, D. Leblanc, T. McDermid, I. S. Jaffe, D. Gao, R. Stith, J. Ryerson, T. Aikin, K. Campos, T. Weinheimer, A. Avery, M. A. Increasing springtime ozone mixing ratios in the free troposphere over western North America. Nature 2010; 463: 344-348.

Cooper OR, Langford AO, Parrish DD, Fahey DW. Challenges of a lowered U.S. ozone standard. Science 2015; 348: 1096-1097.

Cooper OR, Oltmans SJ, Johnson BJ, Brioude J, Angevine W, Trainer M, et al. Measurement of western U.S. baseline ozone from the surface to the tropopause and assessment of downwind impact regions. Journal of Geophysical Research: Atmospheres 2011; 116: D00V03.

Dempsey F. Observations of stratospheric O3 intrusions in air quality monitoring data in Ontario, Canada. Atmospheric Environment 2014; 98: 111-122.

Doe BR. Lead Isotopes: Springer-Verlag Berlin Heidelberg, 1970.

Draxler RR, Hess GD. Description of the HYSPLIT_4 modeling system. NOAA Technical Memorandum ERL ARL-224, 1997, pp. 24.

Díaz-Somoano M, Kylander ME, López-Antón MA, Suárez-Ruiz I, Martínez-Tarazona MR, Ferrat M, et al. Stable Lead Isotope Compositions In Selected Coals From Around The World And Implications For Present Day Aerosol Source Tracing. Environmental Science & Technology 2009; 43: 1078-1085.

EPA USEPA. Exceptional events documents ozone - Washoe, NV. 2017, 2017.

European Commission. Air Quality Standards. 2017, 2016.

900 Ewing SA, Christensen JN, Brown ST, Vancuren RA, Cliff SS, Depaolo DJ. Pb Isotopes as an Indicator of the
901 Asian Contribution to Particulate Air Pollution in Urban California. Environmental Science &
902 Technology 2010; 44: 8911-8916.
903 Fine R, Miller MB, Burley J, Jaffe DA, Pierce RB, Lin M, et al. Variability and sources of surface ozone at
904 rural sites in Nevada, USA: Results from two years of the Nevada Rural Ozone Initiative. Science
905 of The Total Environment 2014.
906 Fine R, Miller MB, Burley J, Jaffe DA, Pierce RB, Lin M, et al. Variability and sources of surface ozone at
907 rural sites in Nevada, USA: Results from two years of the Nevada Rural Ozone Initiative. Science
908 of The Total Environment 2015a; 530–531: 471-482.
909 Fine R, Miller MB, Yates EL, Iraci LT, Gustin MS. Investigating the influence of long-range transport on
910 surface O3 in Nevada, USA, using observations from multiple measurement platforms. Science
911 of The Total Environment 2015b; 530–531: 493-504.
912 Finlayson-Pitts BJ, Pitts Jr JN. Chapter 4 - Photochemistry of Important Atmospheric Species. In:
913 Finlayson-Pitts BJ, Pitts JN, editors. Chemistry of the Upper and Lower Atmosphere. Academic
914 Press, San Diego, 2000a, pp. 86-129.
915 Finlayson-Pitts BJ, Pitts Jr JN. Chapter 14 - Global Tropospheric Chemistry and Climate Change. In:
916 Finlayson-Pitts BJ, Pitts JN, editors. Chemistry of the Upper and Lower Atmosphere. Academic
917 Press, San Diego, 2000b, pp. 762-843.
918 Fiore A, Jacob DJ, Liu H, Yantosca RM, Fairlie TD, Li Q. Variability in surface ozone background over the
919 United States: Implications for air quality policy. Journal of Geophysical Research: Atmospheres
920 2003; 108: 4787.
921 Fiore AM, Jacob DJ, Bey I, Yantosca RM, Field BD, Fusco AC, et al. Background ozone over the United
922 States in summer: Origin, trend, and contribution to pollution episodes. Journal of Geophysical
923 Research: Atmospheres 2002; 107: ACH 11-1-ACH 11-25.
924 Fiore AM, Oberman JT, Lin MY, Zhang L, Clifton OE, Jacob DJ, et al. Estimating North American
925 background ozone in U.S. surface air with two independent global models: Variability,
926 uncertainties, and recommendations. Atmospheric Environment 2014; 96: 284-300.
927 Gratz LE, Jaffe DA, Hee JR. Causes of increasing ozone and decreasing carbon monoxide in springtime at
928 the Mt. Bachelor Observatory from 2004 to 2013. Atmospheric Environment 2015; 109: 323-
929 330.
930 Gustin MS, Amos HM, Huang J, Miller MB, Heidecorn K. Successes and challenges of measuring and
931 modeling atmospheric mercury at the part per quadrillion level: a critical review. Atmos. Chem.
932 Phys. Discuss. 2015a; 15: 3777-3821.
933 Gustin MS, Fine R, Miller M, Jaffe D, Burley J. The Nevada Rural Ozone Initiative (NVROI): Insights to
934 understanding air pollution in complex terrain. Science of The Total Environment 2015b; 530–
935 531: 455-470.
936 Gustin MS, Huang J, Miller MB, Peterson C, Jaffe DA, Ambrose J, et al. Do We Understand What the
937 Mercury Speciation Instruments Are Actually Measuring? Results of RAMIX. Environmental
938 Science & Technology 2013; 47: 7295-7306.
939 Gustin MS, Pierce AM, Huang J, Miller MB, Holmes H, Loria-Salazar SM. Evidence for different reactive
940 Hg sources and chemical compounds at adjacent valley and high elevation locations.
941 Environmental Science & Technology 2016.
942 Hopper JF, Ross HB. Regional source discrimination of atmospheric aerosols in Europe using the isotopic
943 composition of lead. Tellus B 1991; 43: 45-60.
944 Huang J, Gustin MS. Uncertainties of Gaseous Oxidized Mercury Measurements Using KCl-Coated
945 Denuders, Cation-Exchange Membranes, and Nylon Membranes: Humidity Influences.
946 Environmental Science & Technology 2015; 49: 6102-6108.

947 Huang J, Miller MB, Weiss-Penzias P, Gustin MS. Comparison of Gaseous Oxidized Hg Measured by KCl-
948 Coated Denuders, and Nylon and Cation Exchange Membranes. Environmental Science &
949 Technology 2013; 47: 7307-7316.
950 Jacob DJ, Logan JA, Murti PP. Effect of rising Asian emissions on surface ozone in the United States.
951 Geophysical Research Letters 1999; 26: 2175-2178.
952 Jaffe D, Anderson T, Covert D, Kotchenruther R, Trost B, Danielson J, et al. Transport of Asian air
953 pollution to North America. Geophysical Research Letters 1999; 26: 711-714.
954 Jaffe D, Bertschi I, Jaeglé L, Novelli P, Reid JS, Tanimoto H, et al. Long-range transport of Siberian
955 biomass burning emissions and impact on surface ozone in western North America. Geophysical
956 Research Letters 2004; 31: n/a-n/a.
957 Jaffe D, Mahura A, Kelley J, Atkins J, Novelli PC, Merrill J. Impact of Asian emissions on the remote North
958 Pacific atmosphere: Interpretation of CO data from Shemya, Guam, Midway and Mauna Loa.
959 Journal of Geophysical Research: Atmospheres 1997; 102: 28627-28635.
960 Jaffe D, McKendry I, Anderson T, Price H. Six 'new' episodes of trans-Pacific transport of air pollutants.
961 Atmospheric Environment 2003; 37: 391-404.
962 Jaffe D, Prestbo E, Swartzendruber P, Weiss-Penzias P, Kato S, Takami A, et al. Export of atmospheric
963 mercury from Asia. Atmospheric Environment 2005; 39: 3029-3038.
964 Jaffe DA, Lyman S, Amos HM, Gustin MS, Huang J, Selin NE, et al. Progress on Understanding
965 Atmospheric Mercury Hampered by Uncertain Measurements. Environmental Science &
966 Technology 2014; 48: 7204-7206.
967 Johnson WB, Viezee W. Stratospheric ozone in the lower troposphere —I. Presentation and
968 interpretation of aircraft measurements. Atmospheric Environment (1967) 1981; 15: 1309-1323.
969 Jones CE, Halliday AN, Rea DK, Owen RM. Eolian inputs of lead to the North Pacific. Geochimica et
970 Cosmochimica Acta 2000; 64: 1405-1416.
971 Knowland KE, Doherty RM, Hodges KI. The effects of springtime mid-latitude storms on trace gas
972 composition determined from the MACC reanalysis. Atmos. Chem. Phys. 2015; 15: 3605-3628.
973 Komárek M, Ettler V, Chrastný V, Mihaljevič M. Lead isotopes in environmental sciences: A review.
974 Environment International 2008; 34: 562-577.
975 Kunz H, Speth P. Variability of Near-Ground Ozone Concentrations During Cold Front Passages – a
976 Possible Effect of Tropopause Folding Events. Journal of Atmospheric Chemistry 1997; 28: 77-95.
977 Langford AO, Brioude J, Cooper OR, Senff CJ, Alvarez RJ, Hardesty RM, et al. Stratospheric influence on
978 surface ozone in the Los Angeles area during late spring and early summer of 2010. Journal of
979 Geophysical Research: Atmospheres 2012; 117: n/a-n/a.
980 Langford AO, Pierce RB, Schultz PJ. Stratospheric intrusions, the Santa Ana winds, and wildland fires in
981 Southern California. Geophysical Research Letters 2015a; 42: 6091-6097.
982 Langford AO, Senff CJ, Alvarez Ii RJ, Brioude J, Cooper OR, Holloway JS, et al. An overview of the 2013 Las
983 Vegas Ozone Study (LVOS): Impact of stratospheric intrusions and long-range transport on
984 surface air quality. Atmospheric Environment 2015b; 109: 305-322.
985 Langford AOaARJaBJaFRaGMSaLMYaMRD. Entrainment of stratospheric air and Asian pollution by the
986 convective boundary layer in the southwestern U.S. Journal of Geophysical Research:
987 Atmospheres 2017: n/a--n/a.
988 Li Q, Cheng H, Zhou T, Lin C, Guo S. The estimated atmospheric lead emissions in China, 1990–2009.
989 Atmospheric Environment 2012; 60: 1-8.
990 Lin M, Fiore AM, Horowitz LW, Cooper OR, Naik V, Holloway J, et al. Transport of Asian ozone pollution
991 into surface air over the western United States in spring. Journal of Geophysical Research:
992 Atmospheres 2012; 117: D00V07.

Lin M, Fiore AM, Horowitz LW, Langford AO, Oltmans SJ, Tarasick D, et al. Climate variability modulates western US ozone air quality in spring via deep stratospheric intrusions. Nature Communications 2015; 6: 7105.
Lu X, Zhang L, Yue X, Zhang J, Jaffe DA, Stohl A, et al. Wildfire influences on the variability and trend of summer surface ozone in the mountainous western United States. Atmos. Chem. Phys. 2016; 16: 14687-14702.
Lyman SN, Jaffe DA. Formation and fate of oxidized mercury in the upper troposphere and lower stratosphere. Nature Geoscience 2012; 5: 114-117.
Miller MB, Fine R, Pierce AM, Gustin MS. Identifying sources of ozone to three rural locations in Nevada, USA, using ancillary gas pollutants, aerosol chemistry, and mercury. Science of The Total Environment 2015; 530–531: 483-492.
Parmar RS, Welling M, Andreae MO, Helas G. Water vapor release from biomass combustion. Atmos. Chem. Phys. 2008; 8: 6147-6153.
Pierce AM, Gustin MS. Development of a Particulate Mass Measurement System for Quantification of Ambient Reactive Mercury. Environmental Science & Technology 2016.
Pierce AM, Gustin MS. Development of a Particulate Mass Measurement System for Quantification of Ambient Reactive Mercury. Environmental Science & Technology 2017; 51: 436-445.
Price HU, Jaffe DA, Cooper OR, Doskey PV. Photochemistry, ozone production, and dilution during long-range transport episodes from Eurasia to the northwest United States. Journal of Geophysical Research: Atmospheres 2004; 109: n/a-n/a.
Prinn RG. 5.1 - Ozone, Hydroxyl Radical, and Oxidative Capacity. In: Holland HD, Turekian KK, editors. Treatise on Geochemistry (Second Edition). Elsevier, Oxford, 2014, pp. 1-18.
Reinemann SA, Porinchu DF, Gustin MS, Mark BG. Historical trends of mercury and spheroidal carbonaceous particle deposition in sub-alpine lakes in the Great Basin, United States. Journal of Paleolimnology 2014; 52: 405-418.
Rieder HE, Frossard L, Ribatet M, Staehelin J, Maeder JA, Di Rocco S, et al. On the relationship between total ozone and atmospheric dynamics and chemistry at mid-latitudes - Part 2: The effects of the El Niño/Southern Oscillation, volcanic eruptions and contributions of atmospheric dynamics and chemistry to long-term total ozone changes. Atmospheric Chemistry and Physics 2013; 13: 165-179.
Schroeder WH, Munthe J. Atmospheric mercury - An overview. Atmospheric Environment 1998; 32: 809-822.
Stohl A. Computation, accuracy and applications of trajectories—A review and bibliography. Atmospheric Environment 1998; 32: 947-966.
Stohl A, Eckhardt S, Forster C, James P, Spichtinger N, Seibert P. A replacement for simple back trajectory calculations in the interpretation of atmospheric trace substance measurements. Atmospheric Environment 2002; 36: 4635-4648.
Stohl A, Forster C, Eckhardt S, Spichtinger N, Huntrieser H, Heland J, et al. A backward modeling study of intercontinental pollution transport using aircraft measurements. Journal of Geophysical Research: Atmospheres 2003; 108: n/a-n/a.
Stohl A, Spichtinger-Rakowsky N, Bonasoni P, Feldmann H, Memmesheimer M, Scheel HE, et al. The influence of stratospheric intrusions on alpine ozone concentrations. Atmospheric Environment 2000; 34: 1323-1354.
Tan MG, Zhang GL, Li XL, Zhang YX, Yue WS, Chen JM, et al. Comprehensive Study of Lead Pollution in Shanghai by Multiple Techniques. Analytical Chemistry 2006; 78: 8044-8050.
Tang Q, Prather MJ. Correlating tropospheric column ozone with tropopause folds: the Aura-OMI satellite data. Atmospheric Chemistry and Physics 2010; 10: 9681-9688.

TAPI TAPI. Operation Manula: Model 602 BETA PLUS particle measurement system. Teledyne Advanced Pollution Instrumentation, San Diego, CA, 2012, pp. 180.
Teakles AD, So R, Ainslie B, Nissen R, Schiller C, Vingarzan R, et al. Impacts of the July 2012 Siberian fire plume on air quality in the Pacific Northwest. Atmos. Chem. Phys. 2017; 17: 2593-2611.
Timonen H, Ambrose JL, Jaffe DA. Oxidation of elemental Hg in anthropogenic and marine airmasses. Atmos. Chem. Phys. 2013; 13: 2827-2836.
U.S. Energy Information Administration. Coal. Quarterly Coal Report 2015. 2017. U.S. Department of Energy, 2017.
U.S. EPA USEPA. Ozone, 2013.
UNEP. Minamata Convention on Mercury. 2017, 2017.
VanCuren R. Transport aloft drives peak ozone in the Mojave Desert. Atmospheric Environment 2015; 109: 331-341.
VanCuren R, Gustin MS. Identification of sources contributing to PM2.5 and ozone at elevated sites in the western U.S. by receptor analysis: Lassen Volcanic National Park, California, and Great Basin National Park, Nevada. Science of The Total Environment 2015; 530–531: 505-518.
VanCuren RA. Asian aerosols in North America: Extracting the chemical composition and mass concentration of the Asian continental aerosol plume from long-term aerosol records in the western United States. Journal of Geophysical Research: Atmospheres 2003; 108: 4623.
VanCuren RA, Cliff SS, Perry KD, Jimenez-Cruz M. Asian continental aerosol persistence above the marine boundary layer over the eastern North Pacific: Continuous aerosol measurements from Intercontinental Transport and Chemical Transformation 2002 (ITCT 2K2). Journal of Geophysical Research: Atmospheres 2005; 110: D09S90.
Viezee W, Johnson WB, Singh HB. Stratospheric ozone in the lower troposphere—II. Assessment of downward flux and ground-level impact. Atmospheric Environment (1967) 1983; 17: 1979-1993.
Vingarzan R. A review of surface ozone background levels and trends. Atmospheric Environment 2004; 38: 3431-3442.
Weiss-Penzias P, Jaffe D, Swartzendruber P, Hafner W, Chand D, Prestbo E. Quantifying Asian and biomass burning sources of mercury using the Hg/CO ratio in pollution plumes observed at the Mount Bachelor observatory. Atmospheric Environment 2007; 41: 4366-4379.
Weiss-Penzias P, Jaffe DA, McClintick A, Prestbo EM, Landis MS. Gaseous Elemental Mercury in the Marine Boundary Layer: Evidence for Rapid Removal in Anthropogenic Pollution. Environmental Science & Technology 2003; 37: 3755-3763.
Weiss-Penzias P, Jaffe DA, Swartzendruber P, Dennison JB, Chand D, Hafner W, et al. Observations of Asian air pollution in the free troposphere at Mount Bachelor Observatory during the spring of 2004. J. Geophys. Res. 2006; 111: D10304.
Weiss-Penzias PA, H. M. Selin, N. E. Gustin, M. S. Jaffe, D. A. Obrist, D. Sheu, G.-R. Giang, A. Use of a global model to understand speciated atmospheric mercury observations at five high-elevation sites. Atmospheric Chemistry and Physics 2015; 15: 1161-1173.
Wilkening KE, Barrie LA, Engle M. Trans-Pacific Air Pollution. Science 2000; 290: 65.
Zhang L, Jacob DJ, Downey NV, Wood DA, Blewitt D, Carouge CC, et al. Improved estimate of the policy-relevant background ozone in the United States using the GEOS-Chem global model with 1/2° × 2/3° horizontal resolution over North America. Atmospheric Environment 2011; 45: 6769-6776.
Zhang L, Jacob DJ, Yue X, Downey NV, Wood DA, Blewitt D. Sources contributing to background surface ozone in the US Intermountain West. Atmos. Chem. Phys. 2014; 14: 5295-5309.